Speckle Observations of TESS Exoplanet Host Stars. II. Stellar Companions at 1-1000 AU and Implications for Small Planet Detection

Kathryn V. Lester,[1] Rachel A. Matson,[2] Steve B. Howell,[1] Elise Furlan,[3] Crystal L. Gnilka,[1] Nicholas J. Scott,[1] David R. Ciardi,[3] Mark E. Everett,[4] Zachary D. Hartman,[5,6] and Lea A. Hirsch[7]

[1]NASA Ames Research Center, Moffett Field, CA 94035, USA
[2]U.S. Naval Observatory, Washington, D.C. 20392, USA
[3]NASA Exoplanet Science Institute, Caltech/IPAC, Pasadena, CA 91125, USA
[4]NSF's National Optical-Infrared Astronomy Research Laboratory, Tucson, AZ 85719, USA
[5]Lowell Observatory, Flagstaff, AZ 86001, USA
[6]Department of Physics & Astronomy, Georgia State University, Atlanta GA 30303, USA
[7]Kavli Institute for Particle Astrophysics and Cosmology, Stanford University, Stanford, CA 94305, USA

ABSTRACT

We present high angular resolution imaging observations of 517 host stars of TESS exoplanet candidates using the 'Alopeke and Zorro speckle cameras at Gemini North and South. The sample consists mainly of bright F, G, K stars at distances of less than 500 pc. Our speckle observations span angular resolutions of ∼20 mas out to 1.2 arcsec, yielding spatial resolutions of <10 to 500 AU for most stars, and our contrast limits can detect companion stars $5-9$ magnitudes fainter than the primary at optical wavelengths. We detect 102 close stellar companions and determine the separation, magnitude difference, mass ratio, and estimated orbital period for each system. Our observations of exoplanet host star binaries reveal that they have wider separations than field binaries, with a mean orbital semi-major axis near 100 AU. Other imaging studies have suggested this dearth of very closely separated binaries in systems which host exoplanets, but incompleteness at small separations makes it difficult to disentangle unobserved companions from a true lack of companions. With our improved angular resolution and sensitivity, we confirm that this lack of close exoplanet host binaries is indeed real. We also search for a correlation between planetary orbital radii vs. binary star separation, but given the very short orbital periods of the TESS planets, we do not find any clear trend. We do note that in exoplanet systems containing binary host stars, there is an observational bias against detecting Earth-size planet transits due to transit depth dilution caused by the companion star.

1. INTRODUCTION

The Kepler, K2, and TESS missions have provided precise, light curve photometry for millions of stars and contributed breakthrough advancements in many fields of stellar astrophysics (Borucki et al. 2010; Howell et al. 2014; Ricker et al. 2015). This includes the discovery of thousands of extra-solar planets through the transit method, where a planet passing in front of a star causes a periodic dip in brightness. Due to the large pixel sizes of 4" for Kepler/K2 and 21" for TESS, nearby stars or unresolved stellar companions within the aperture dilute the transit depth and bias the measured planet radius (Ciardi et al. 2015). About 50% of solar-type exoplanet hosts have companions (e.g., Horch et al. 2014; Matson et al. 2018), so follow-up high resolution imaging is needed to search for unresolved companions and aid exoplanet validation and characterization.

Understanding how binary companions affect the formation, evolution, and survival of exoplanets is also an important component to understanding planet formation overall. Theoretical studies show that a companion can truncate the protoplanetary disk, leaving less

Corresponding author: Kathryn Lester
kathryn.v.lester@nasa.gov

material for planets to form (Martin et al. 2014; Jang-Condell 2015), cause the migration of gas giant planets (Dawson & Johnson 2018), or disperse the disk before planets are able to form (Cieza et al. 2009; Kraus et al. 2012). Observational studies using high resolution imaging (Kraus et al. 2016; Fontanive et al. 2019; Ziegler et al. 2020, 2021; Howell et al. 2021) and radial velocities (Wang et al. 2014; Hirsch et al. 2021) have found fewer companions within 100 AU around exoplanet hosts than around field stars, supporting the idea that close stellar companions do suppress planet formation.

However, it is difficult to disentangle unobserved companions from a true lack of companions without sufficient angular resolution. The angular separations of the closest companions (< 50 AU) around Kepler exoplanet hosts are near or below the diffraction limit of most telescopes, but TESS observed brighter, nearby stars for which we can resolve companions at smaller physical separations from the host star. We present the highest angular resolution speckle images of TESS exoplanet host stars in search of companions at $1 - 100$ AU where planet formation would be greatly hindered. We describe our observations and companion detections in Section 2, then create a simulated sample of binary stars to investigate the separation distribution of exoplanet host binaries in Section 3. Our results and conclusions are presented in Sections 4 and 5, respectively.

2. OBSERVATIONS

2.1. *Speckle Imaging*

We observed 517 stars from the TESS Objects of Interest (TOI) catalog using the 'Alopeke and Zorro speckle cameras (Scott et al. 2018, 2021) on the Gemini 8.1 m North and South telescopes respectively from May 2019 to December 2020. Before each observing season, targets were selected from the latest version of the TOI catalog of likely planet candidates. All of our observations are listed in Tables 3 and 4 in the Appendix, with the TOI and TIC numbers, TESS magnitude, UT date, the inverse of the parallax from Gaia EDR3 (Gaia Collaboration et al. 2016, 2020) for the distance, effective temperature of the host star from the TESS Input Catalog (TIC v8.1, Stassun et al. 2019), and notes for each target. The Julian date of each observation can be found in the headers of the archival data hosted on the Gemini Observatory Archive[1]. At least three image sets were obtained for each target, where one set consists of 1000 60 ms exposures taken in a 562 nm and an 832 nm filter simultaneously. Additional image sets were taken

for fainter targets ($V > 9$ mag), and a point source standard star was observed immediately before or after each target for calibration.

The data were reduced using the pipeline developed by the speckle team (Howell et al. 2011; Horch et al. 2011) to calculate and average the power spectrum of each image, then correct for the speckle transfer function by dividing the mean power spectrum of the target by that of the standard star. The pipeline also produces a reconstructed image of each target with a field of view of 1.3" in radius around the target. The contrast limits for each target were determined with the method described in Horch et al. (2011), which uses the background flux levels to determine the faintest companions one could reliably detect at each separation. These 5σ contrast limits at $0.2''$ and $1.0''$ in the blue and red filters are also listed in Tables 3 and 4.

Due to the large TESS pixels, some transit detections were identified to be false positives through follow-up photometry. If the light curve shows chromaticity or v-shaped dips of alternating depth, the event must be a binary eclipse rather than a planet transit, then confirmed with follow-up observations to identify the eclipsing source within the TESS aperture. The transits for 105 of the TOI's in our sample have been identified as false positives (or false alarms) on the Exoplanet Follow-up Observing Program (ExoFOP)[2] website, noted in Tables 3 and 4. We have eliminated these host stars from further consideration here, leaving us with 412 stars. A few additional systems were classified as ambiguous planetary candidates (APC), for example, if only a single transit was observed. Because these systems have not yet been confirmed as false positives, we kept them in our sample and discuss their impact in Section 4.1.

Figure 1 shows the distributions in effective temperature, distance, and TESS magnitude for our 412 exoplanet host TOI's. Our sample contains primarily bright, Solar-type stars with smaller distances from Earth compared to Kepler host stars, allowing Gemini speckle observations to detect companions quite close to the target star. For distances of $100 - 500$ pc, our inner angular resolution of 0.017" at 562 nm corresponds to separations of $1.7 - 8.5$ AU, while our inner angular resolution of 0.026" at 832 nm corresponds to separations of $2.6 - 13.0$ AU. Therefore, we can successfully detect stellar companions in the $1 - 100$ AU regime and determine their properties.

[2] https://exofop.ipac.caltech.edu/tess

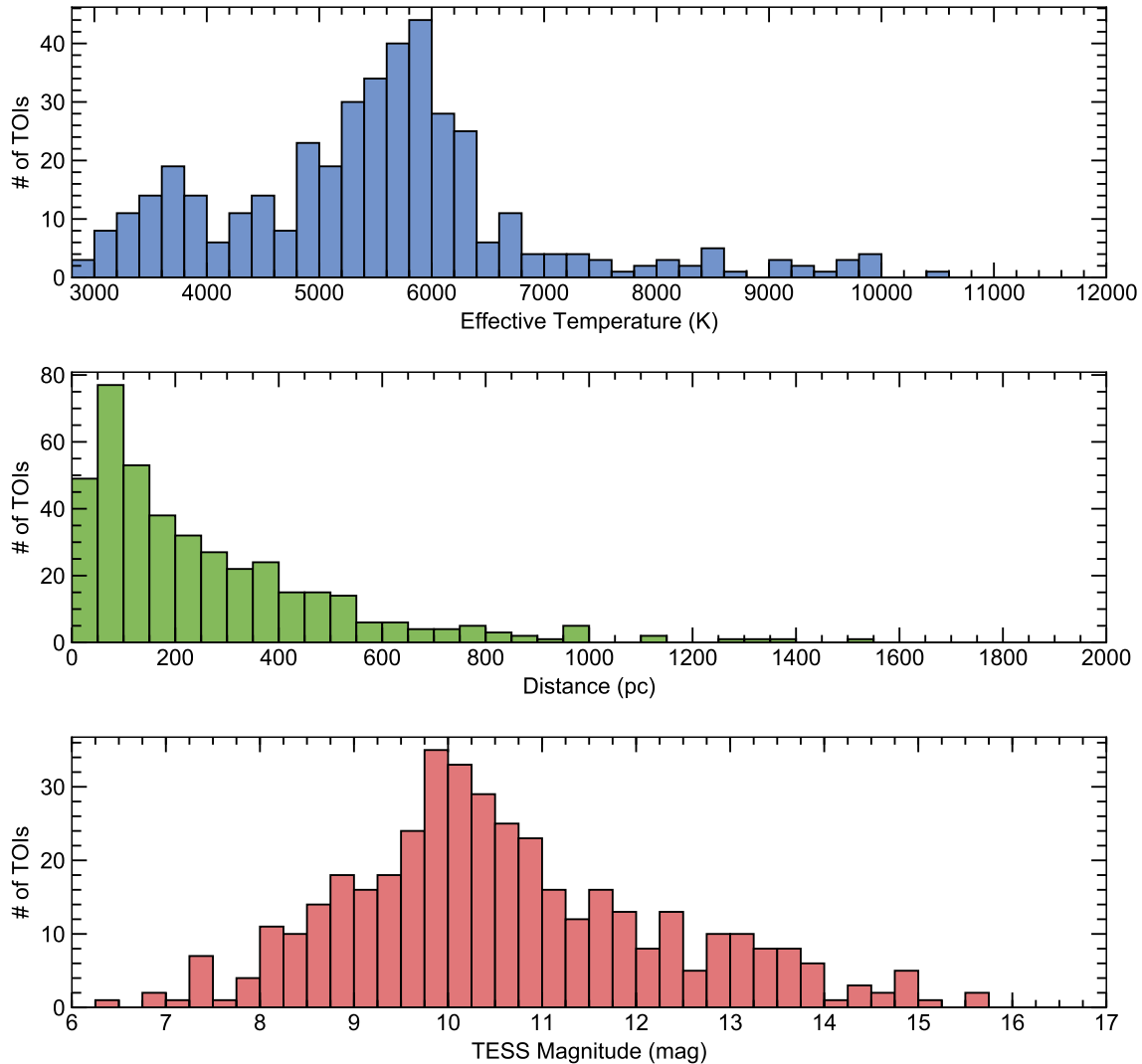[1] https://archive.gemini.edu/searchform

Figure 1. Stellar parameter distributions for the 412 exoplanet host TOI's in our sample, including stellar effective temperature (top), Gaia EDR3 distance (middle), and TESS magnitude (bottom).

2.2. *Detected Companions*

Binary stars produce a characteristic interference fringe pattern in the power spectrum from which the companion's angular separation (ρ), position angle (θ, measured East of North), and magnitude difference (Δm) can be determined from a weighted least squares fit. Figure 2 shows an example contrast curve and reconstructed image for the binary star TOI 1343. We detected a total of 102 stellar companions around 99 TOI's in our sample: 73 companions around exoplanet host stars and 29 companions around transit false positive stars. Our results are listed in Table 1 for both the exoplanet candidate host stars and the false positive stars, with the TOI number, observation date, and companion parameters ($\rho, \theta, \Delta m$) determined from both the 562 nm and 832 nm images. We detected some companions only

in the 832 nm filter, and could not constrain the magnitude difference for three of these systems. Results from multiple nights were averaged together because no orbital motion could be seen, so any TOI's with duplicate entries in Table 1 were found to be triple systems. The typical uncertainties in the separation, position angle, and magnitude difference are 0.01", 0.5 degrees, and 0.5 mag, respectively.

Several of these companions were previously detected by the NESSI speckle camera on the WIYN 3.5 m telescope (Howell et al. 2021) or HRCam on the SOAR 4.1 m telescope (Ziegler et al. 2020). Most separations and position angles from Gemini agree with those from WIYN and SOAR at the 1σ level. One exception was TOI 1191, for which a companion was found at $\rho = 0.68$" with $\Delta m = 5$ mag by 'Alopeke but at $\rho = 0.046$" with $\Delta m = 1.54$ mag by NESSI. Palomar adaptive optics ob-
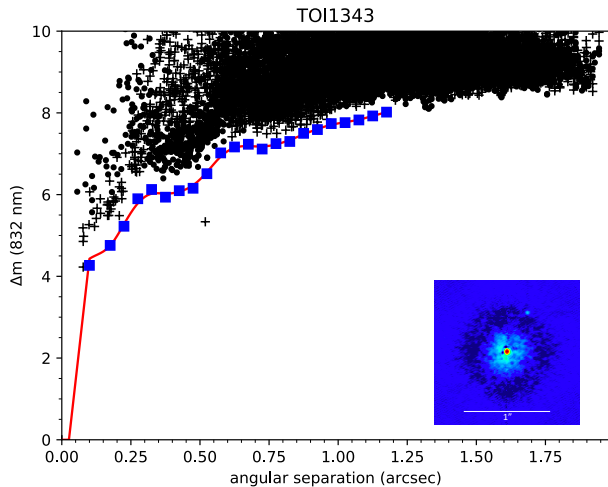
Figure 2. Example detection limit as a function of radius from the center for a binary star (TOI 1343). The black points represent the local maxima (crosses) and minima (dots). The blue squares mark the 5σ background sensitivity limit within 0.05" bins, and the red line corresponds to a spline fit. A companion is detected if any maxima points lie below the detection limit, such as the point near 0.5" in this example. The inset plot shows the reconstructed image where the companion is visible in the top right (northwest) corner.

servations also found a companion at 0.5", consistent with the 'Alopeke results. This TOI could be a triple system, but future observations at higher signal-to-noise are needed to confirm these companions.

Due to speckles becoming de-correlated at 1.2", companions beyond this limit have larger uncertainties, especially in Δm. These wide companions are also more likely to be line-of-sight companions, rather than gravitationally bound systems (Horch et al. 2014; Matson et al. 2018), but this can be confirmed with Gaia proper motion and parallaxes (e.g., Mugrauer & Michel 2020). We do not consider these wide companions nor the companions around transit false positive TOI's in the rest of our analysis. Figure 3 shows the magnitude difference versus angular separation for the remaining 58 companions with $\rho < 1.2$" as well as our typical detection limit. We also chose to include the companions detected at WIYN in our analysis to increase our sample size; Howell et al. (2021) observed an additional 130 Solar-type TOI's and detected 18 companions with separations less than 1.2" that are included in our comparison of exoplanet host binaries and field binaries in Section 4.1. This final sample only includes binaries, as no triple systems with separations less than 1.2" were detected.

2.3. *Binary Properties*

We estimated the mass ratio (M_2/M_1) of each detected binary system using the method in Matson et

al. (2019) and Howell et al. (2021). For each primary star, we found the nearest value in the Modern Mean Dwarf Stellar Color and Effective Temperature Sequence (Pecaut & Mamajek 2013) based on the effective temperature, then calculated the V-band magnitude differences (Δm_V) of all possible companions (stars with cooler effective temperatures). For companions detected in our 562 nm filter, we fit a polynomial to the mass ratio as a function of Δm_V then calculated the mass ratio corresponding to the observed magnitude difference. For companions detected in the 832 nm filter, we converted the magnitude differences from the V-band to the TESS band (Δm_{TESS}) using the relations in Stassun et al. (2018), then interpolated the mass ratio from the polynomial fit. We took the average if a companion was detected in both filters, then estimated a typical uncertainty of 0.02 from the difference in the mass ratio across filters. Our results are listed in Table 1, and Figure 4 shows the mass ratio as a function of magnitude difference for select binaries and a histogram of the mass ratios. Our sample of exoplanet host binaries does not show the peak towards $M_2/M_1 = 1$ seen in field binaries, possibly because our binaries have long orbital periods that do not show a preference for equal mass components (Raghavan et al. 2010).

Next, we calculated the separation in AU from the angular separation and the Gaia distance for each system, shown in the right panel of Figure 3. We then estimated the binary orbital period using Kepler's Third Law, the primary component's mass estimated from the effective temperature, the secondary component's mass calculated from the mass ratio, and the semi-major axis equal to the instantaneous separation measured with our speckle observations. This last assumption is discussed further in Section 3.3. The estimated semi-major axes and orbital periods are listed in the last columns of Table 1. Figure 5 shows the logarithmic distribution of companion separation broken down by spectral type of the primary star. The distributions look similar for all spectral types, except the M-stars for which we only detected two companions. This is likely due to their decreased multiplicity rate (27%) and the smaller peak separation (20 AU) of M-type field binaries (Winters et al. 2019), so most close companions could not be resolved by speckle interferometry. These stars are also quite faint, so our observations may not have achieved sufficiently deep contrast limits to detect fainter companions. For our comparison with different model predictions, we only consider binaries with an F-, G-, or K-type primary (47 systems), which make up the majority of our sample.
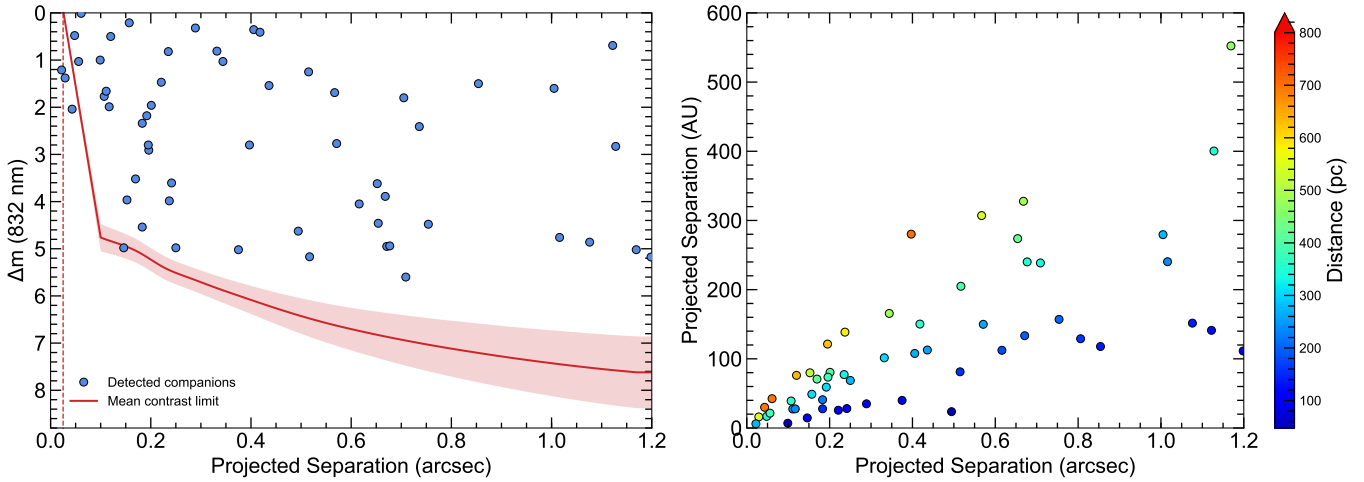
Figure 3. Properties of the 58 companions with separations less than 1.2" around exoplanet host stars. *Left:* The magnitude difference as a function of the angular separation. The detected companions are shown as the solid blue points. The average 5σ detection limit is shown as the solid red line, and the shading corresponds to the typical spread in this limit. The few companions below the contrast limit correspond to observations taken during better seeing or at higher signal-to-noise. The Gemini angular resolution limit in the 832 nm filter is shown as the vertical red line. *Right:* Comparison of the observed angular separation of our detected companions and the derived spatial separation determined using Gaia distances. The color corresponds to the system distance.
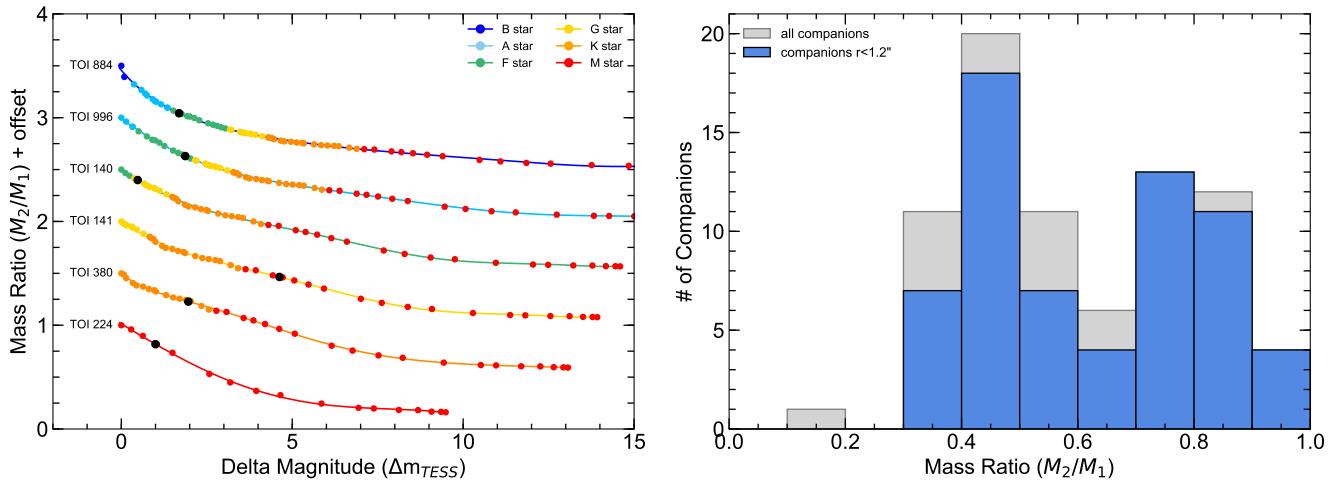
Figure 4. *Left:* Mass ratio as a function of magnitude difference for example exoplanet host binaries. The Pecaut & Mamajek (2013) model values are shown as the colored dots and the polynomial fit for each binary is shown as the solid line; both are color-coded by spectral type of the possible companions and primary star, respectively. The values of the observed companions are shown as the solid black dots. *Right:* Histogram of the mass ratio for exoplanet host stars. The light grey histograms represent all detected companions, while the blue histograms represent companions with separations < 1.2".

Table 1. Companions Detected

Target	ρ ($''$) (562 nm)	θ (deg) (562 nm)	Δm (mag) (562 nm)	ρ ($''$) (832 nm)	θ (deg) (832 nm)	Δm (mag) (832 nm)	M_2/M_1	a (AU)	Binary Period (yr)
				Exoplanet Host Stars					
TOI 140	0.044	336.2	0.76	0.048	337.0	0.48	0.88	16.8	46
TOI 141*	$\cdots$	$\cdots$	$\cdots$	0.494	240.6	4.63	0.47	23.6	93
	$\cdots$	$\cdots$	$\cdots$	1.333	306.8	5.60	0.38	63.7	430
TOI 172	1.175	319.3	5.20	1.262	321.9	5.36	0.43	452.9	7900
TOI 224	0.100	224.8	2.07	0.099	226.6	1.00	0.72	6.9	20
TOI 235	0.850	289.2	1.78	0.854	291.4	1.50	0.75	117.8	1000
TOI 245	0.990	109.1	3.54	1.206	109.6	2.39	0.59	148.3	1300
TOI 252	0.436	307.8	2.16	0.436	309.9	1.54	0.79	112.7	1000
TOI 264	0.655	329.5	5.38	0.654	331.7	4.46	0.45	273.8	3400
TOI 271	$\cdots$	$\cdots$	$\cdots$	0.146	231.1	4.98	0.43	14.6	44
TOI 287	$\cdots$	$\cdots$	$\cdots$	0.152	125.9	3.96	0.52	79.8	570
TOI 291	0.035	146.2	0.65	0.029	145.2	1.38	0.82	16.0	46
TOI 309	0.330	77.6	1.27	0.344	77.7	1.03	0.81	165.6	1700
TOI 325	$\cdots$	$\cdots$	$\cdots$	0.616	221.8	4.05	0.49	112.3	1200
TOI 354	0.054	87.1	1.08	0.056	87.8	1.03	0.82	21.5	73
TOI 364	0.384	95.2	0.36	0.405	96.6	0.35	0.93	107.8	730
TOI 380	$\cdots$	$\cdots$	$\cdots$	0.201	6.1	1.96	0.73	80.4	590
TOI 402	$\cdots$	$\cdots$	$\cdots$	1.467	234.2	9.33	0.14	65.8	540
TOI 457	$\cdots$	$\cdots$	$\cdots$	1.122	223.8	0.69	0.83	141.2	3000
TOI 487	0.515	198.7	1.53	0.515	200.8	1.25	0.77	81.2	570
TOI 492	$\cdots$	$\cdots$	$\cdots$	0.668	321.1	3.89	0.49	327.7	4400
TOI 564	$\cdots$	$\cdots$	$\cdots$	0.671	73.9	4.95	0.44	133.4	1300
TOI 568	0.310	189.8	0.90	0.332	192.0	0.81	0.85	101.5	740
TOI 573	1.442	227.6	1.30	1.600	234.3	1.25	0.69	142.0	2200
TOI 676	$\cdots$	$\cdots$	$\cdots$	1.331	103.8	2.20	0.68	944.1	23300
TOI 680	$\cdots$	$\cdots$	$\cdots$	0.806	331.4	$\cdots$	$\cdots$	129.0	1400
TOI 697*	$\cdots$	$\cdots$	$\cdots$	1.199	137.9	5.17	0.41	111.4	1000
	$\cdots$	$\cdots$	$\cdots$	1.269	139.4	5.46	0.38	117.9	1100
TOI 722	0.224	114.1	2.46	0.221	115.8	1.47	0.72	25.7	120
TOI 791	$\cdots$	$\cdots$	$\cdots$	0.709	25.6	5.60	0.37	238.6	2700
TOI 798	0.289	179.4	0.64	0.289	181.5	0.32	0.93	35.0	180
TOI 854	0.023	204.6	1.35	0.022	211.1	1.21	0.79	6.1	11
TOI 906	1.294	49.0	3.67	1.375	50.7	2.98	0.57	186.2	1900
TOI 926	0.192	156.9	2.53	0.192	158.8	2.18	0.68	59.1	350
TOI 931	0.113	234.9	0.65	0.120	237.6	0.50	0.90	76.1	460
TOI 952*	$\cdots$	$\cdots$	$\cdots$	0.169	72.1	3.52	0.48	70.7	390
	$\cdots$	$\cdots$	$\cdots$	1.262	135.4	4.91	0.39	526.3	8300

Table 1 *continued*
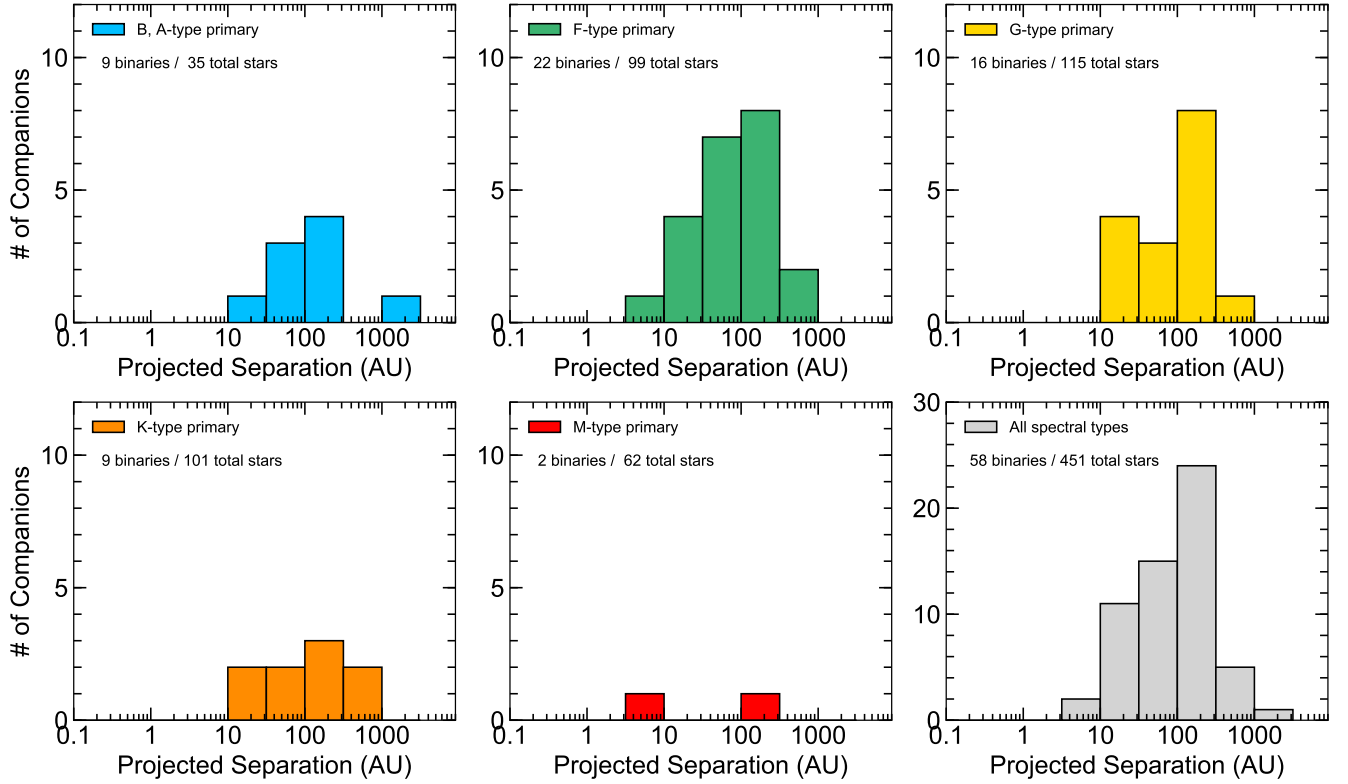
Figure 5. Histograms of the projected physical separation (i.e., semi-major axis) of the exoplanet host binaries in our sample on a logarithmic scale and broken down by the spectral type of the primary star.

Table 1 *(continued)*

Target	ρ $('')$	θ (deg)	Δm (mag)	ρ $('')$	θ (deg)	Δm (mag)	M_2/M_1	a (AU)	Binary
	(562 nm)	(562 nm)	(562 nm)	(832 nm)	(832 nm)	(832 nm)			Period (yr)
TOI 1032	1.161	81.6	2.16	1.329	83.0	1.61	0.59	796.0	11300
TOI 1035	0.101	100.2	1.96	0.107	112.1	1.77	0.71	39.1	180
TOI 1037	⋯	⋯	⋯	0.250	242.1	4.98	0.32	68.7	340
TOI 1039	0.708	285.6	4.02	0.736	286.3	2.41	0.38	1121.6	15500
TOI 1131	0.095	214.4	1.45	0.111	214.0	1.66	0.75	27.5	110
TOI 1133	0.550	102.1	3.05	0.571	102.4	2.77	0.59	149.9	1300
TOI 1152	1.074	22.6	0.93	1.284	22.7	0.85	0.83	133.9	1200
TOI 1189	0.984	318.5	1.36	1.005	319.1	1.60	0.78	279.5	3700
TOI 1191	⋯	⋯	⋯	0.677	85.8	4.94	0.40	240.1	2600
TOI 1192	0.187	200.6	3.37	0.196	201.4	2.91	0.55	73.5	440
TOI 1204	⋯	⋯	⋯	0.375	38.8	5.02	0.39	39.9	180
TOI 1217	1.088	242.7	5.02	1.169	242.7	5.02	0.44	552.3	9700
TOI 1261	⋯	⋯	⋯	1.722	316.9	2.87	0.59	344.2	4900
TOI 1293	⋯	⋯	⋯	1.016	120.4	4.76	0.45	240.4	3000
TOI 1335	0.057	303.1	0.01	0.061	304.1	0.01	0.99	42.4	150

Table 1 *continued*

Table 1 *(continued)*

Target	ρ (″) (562 nm)	θ (deg) (562 nm)	Δm (mag) (562 nm)	ρ (″) (832 nm)	θ (deg) (832 nm)	Δm (mag) (832 nm)	M_2/M_1	a (AU)	Binary Period (yr)
TOI 1343	$\cdots$	$\cdots$	$\cdots$	0.517	333.6	5.17	0.30	204.9	1700
TOI 1440	$\cdots$	$\cdots$	$\cdots$	1.536	324.9	$\cdots$	$\cdots$	363.2	6800
TOI 1447	0.150	67.7	0.22	0.157	67.7	0.21	0.96	48.8	200
TOI 1491	$\cdots$	$\cdots$	$\cdots$	0.754	269.5	4.48	0.47	157.0	1600
TOI 1531	0.565	199.2	1.11	0.567	199.6	1.69	0.82	307.1	4500
TOI 1544	0.624	129.3	3.35	0.652	129.9	3.62	0.58	641.6	15200
TOI 1559	0.039	122.6	2.08	0.043	123.0	2.04	0.61	29.9	92
TOI 1560	1.246	62.7	4.03	1.366	68.4	3.08	0.44	731.2	11400
TOI 1565	0.233	207.3	0.85	0.235	207.7	0.82	0.81	77.2	360
TOI 1598	$\cdots$	$\cdots$	$\cdots$	1.076	304.3	4.86	0.44	151.6	1500
TOI 1636	$\cdots$	$\cdots$	$\cdots$	0.183	356.3	2.34	0.72	27.7	130
TOI 1641	0.194	296.1	3.53	0.195	296.4	2.80	0.46	121.3	730
TOI 1677	$\cdots$	$\cdots$	$\cdots$	0.183	142.0	4.54	0.47	40.9	210
TOI 1678	0.336	307.1	4.01	0.397	307.5	2.80	0.49	280.2	2800
TOI 1719	0.116	193.3	1.78	0.117	193.8	1.99	0.70	27.7	100
TOI 1740	$\cdots$	$\cdots$	$\cdots$	0.241	258.6	3.60	0.56	28.1	130
TOI 2010	$\cdots$	$\cdots$	$\cdots$	1.578	138.0	$\cdots$	$\cdots$	171.1	2200
TOI 2035	0.415	245.9	0.45	0.418	246.2	0.41	0.87	150.2	900
TOI 2220	$\cdots$	$\cdots$	$\cdots$	1.128	251.2	2.83	0.61	400.3	6200
TOI 2305	$\cdots$	$\cdots$	$\cdots$	0.237	203.1	3.98	0.52	138.6	1300
TOI 2310	0.708	332.5	2.81	0.705	334.8	1.80	0.71	650.9	13600
Transit False Positive Stars									
TOI 138	0.099	258.9	1.38	0.108	260.5	1.33	0.78	20.7	94
TOI 146	0.302	75.0	1.15	0.324	77.0	1.15	0.80	161.8	2100
TOI 154	$\cdots$	$\cdots$	$\cdots$	0.154	202.8	1.28	0.77	61.8	470
TOI 311	0.039	130.6	0.91	0.028	148.8	0.96	0.85	6.5	21
TOI 372	$\cdots$	$\cdots$	$\cdots$	0.267	262.3	2.45	0.64	137.8	1600
TOI 378	0.098	167.9	1.29	0.137	182.0	1.49	0.77	316.2	5400
TOI 379	0.053	19.5	0.07	0.052	21.3	0.41	0.95	12.0	41
TOI 463	$\cdots$	$\cdots$	$\cdots$	0.816	214.4	3.78	0.48	150.3	1600
TOI 593	$\cdots$	$\cdots$	$\cdots$	0.664	170.1	3.81	0.49	255.5	3700
TOI 884	0.049	323.2	1.79	0.052	324.1	1.69	0.56	52.7	210
TOI 894	0.619	329.5	3.32	0.649	331.0	2.41	0.49	233.1	2300
TOI 896	$\cdots$	$\cdots$	$\cdots$	0.062	126.2	3.48	0.49	9.6	25
TOI 898	1.306	34.9	2.11	1.358	35.4	2.07	0.70	651.2	16800
TOI 919	0.088	83.7	0.71	0.095	85.9	0.48	0.89	31.4	170
TOI 935	$\cdots$	$\cdots$	$\cdots$	0.785	146.5	2.19	0.74	296.7	5900
TOI 995	0.116	137.9	2.22	0.121	139.5	2.54	0.73	151.1	2100
TOI 996	0.143	228.7	1.99	0.153	230.9	1.87	0.64	79.1	520
TOI 1038	0.443	99.9	1.84	0.474	102.1	1.42	0.66	119.5	910

Table 1 *continued*

Table 1 *(continued)*

Target	ρ (″) (562 nm)	θ (deg) (562 nm)	Δm (mag) (562 nm)	ρ (″) (832 nm)	θ (deg) (832 nm)	Δm (mag) (832 nm)	M_2/M_1	a (AU)	Binary Period (yr)
TOI 1047	0.826	246.4	2.83	0.883	248.7	2.31	0.66	119.5	1300
TOI 1051	0.368	241.0	1.12	0.368	243.1	1.00	0.81	23.2	110
TOI 1093	0.102	108.2	2.21	0.109	110.7	2.04	0.70	64.6	680
TOI 1147	$\cdots$	$\cdots$	$\cdots$	0.377	346.0	3.62	0.51	77.9	620
TOI 1193	0.087	255.3	0.62	0.090	255.4	0.59	0.88	77.9	550
TOI 1417	0.031	307.0	2.71	0.027	307.2	2.63	0.57	4.1	6
TOI 1487	0.097	45.6	4.20	$\cdots$	$\cdots$	$\cdots$	0.55	10.6	39
TOI 1543	$\cdots$	$\cdots$	$\cdots$	0.320	178.5	5.02	0.32	194.4	1800
TOI 1557	$\cdots$	$\cdots$	$\cdots$	1.406	135.7	5.59	0.38	407.3	8200
TOI 1662	0.226	347.4	2.52	0.227	347.5	2.11	0.61	79.3	560
TOI 1673	0.274	50.5	1.61	0.276	50.9	1.50	0.75	58.2	450

[*]Found to be a triple system, so the parameters for each companion are listed separately.

3. SIMULATED BINARIES

3.1. *Field Binary Model*

We simulated a series of binary stars following the methods in Matson et al. (2018) and Ziegler et al. (2020) in order to compare our results to the predictions for field binaries and investigate the suppression of close companions around exoplanet hosts. We began by selecting only F-, G-, and K-type exoplanet candidate hosts from our Gemini TOI sample (337 stars) and the sample observed with WIYN by Howell et al. (2021, 130 stars), then used these masses and distances as the inputs for our simulations. For each of a thousand iterations, we randomly chose 46% of these stars to be the primary components of our simulated binaries following the multiplicity rate of Solar-type field stars found by Raghavan et al. (2010). Masses for the secondary components were then drawn randomly from the distribution in Raghavan et al. (2010): uniform probability for $M_2/M_1 = 0.4 - 0.9$ then a higher probability for $0.9 - 1.0$. The absolute I-band magnitude of each component was interpolated based on mass using the Modern Mean Dwarf Sequence (Pecaut & Mamajek 2013) in order to calculate a magnitude difference for each system.

Next, orbital parameters were randomly assigned to each system from the log-normal period distribution of Raghavan et al. (2010, $\log P = 5.03$ days, $\sigma = 2.28$), the eccentricity distribution of Duquennoy & Mayor (1991), and uniform distributions for the inclination, angular semi-major axis (α), longitude of periastron, and longitude of the ascending node. Finally, we calculated the projected angular separation (ρ) of each companion at a random orbital phase to mimic our speckle observations, then identified "detectable" companions that lie within the Gemini angular resolution (inner) limit of 0.025" and the speckle correlation (outer) limit of 1.2" and have a magnitude difference within the mean 832 nm Gemini contrast limit.

The results of our simulated binary sample are shown in Figure 6. The left panel shows the companion magnitude difference versus separation for several iterations of our simulation, with detectable companions plotted in purple and the undetectable companions plotted in grey. The middle panel shows a histogram of the physical separation on a logarithmic scale for all simulated companions. We averaged the results from each iteration to predict the number of companions detectable with speckle imaging in each 0.5 dex bin, and estimated the uncertainty from the standard deviation across all iterations. This expected number of companions is compared to the observed number in the next section (Section 4.1). We note that WIYN has a slightly larger angular resolution limit and shallower contrast limit than Gemini, and therefore is less sensitive to close companions, but this difference between telescopes is within the simulation's uncertainties. Lastly, the right panel of Figure 6 shows the ratio between the instantaneous separation and the modeled semi-major axis of the detectable companions, which we discuss in Section 3.3.

3.2. *Additional Period Distributions*

Recent work has found that exoplanet host binaries have larger separations than field binaries; for example, Howell et al. (2021) suggests a peak at $\log P = 5.5$ days. We used a grid search to test several different log-
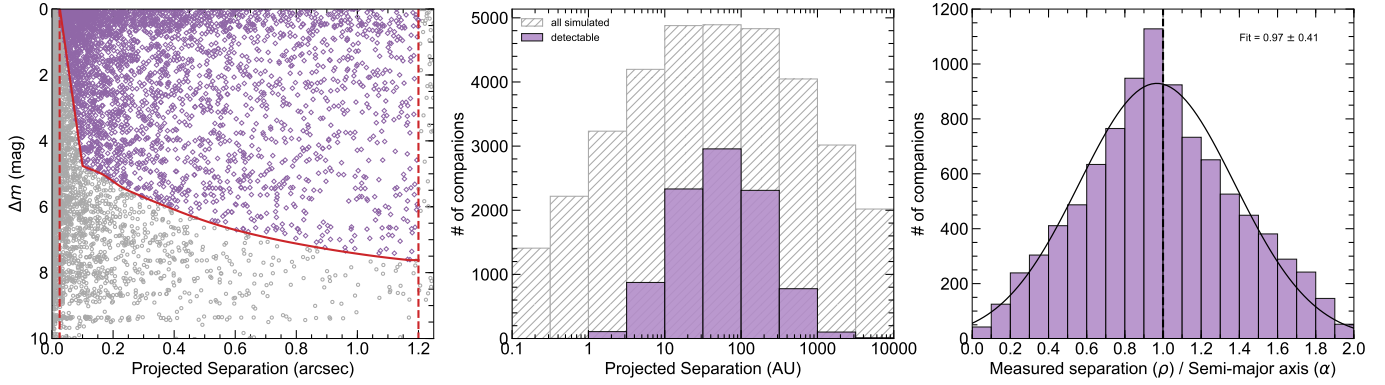
Figure 6. Results of our simulated binary sample based on orbital demographics of field binaries from Raghavan et al. (2010). *Left:* Magnitude difference as a function of the angular separation for a subset of the simulated companions. The detectable companions are shown as purple diamonds, while the undetectable companions are shown as grey circles. The mean Gemini detection limit is shown as the solid red line, and the angular resolution limits are shown as the dashed red lines. *Middle:* Logarithmic distribution of the projected physical separation for the full simulated binary sample. The filled, purple histograms represent the detectable companions, while the grey, hatched histograms represent the full sample. *Right:* Histogram of the ratio between the instantaneous separation and the modeled semi-major axis of the detectable companions. The gaussian fit is shown in solid black, and a dashed line at unity is shown for reference.
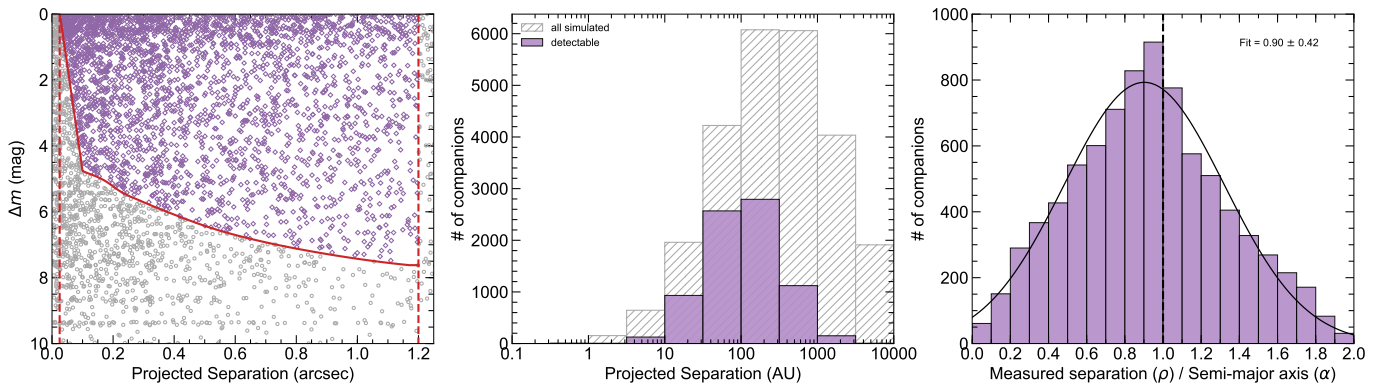
Figure 7. Same as Figure 6, but for simulated binaries created using a log-normal period distribution with the peak at $\log P = 6.2$ days and width of $\sigma = 1.2$.
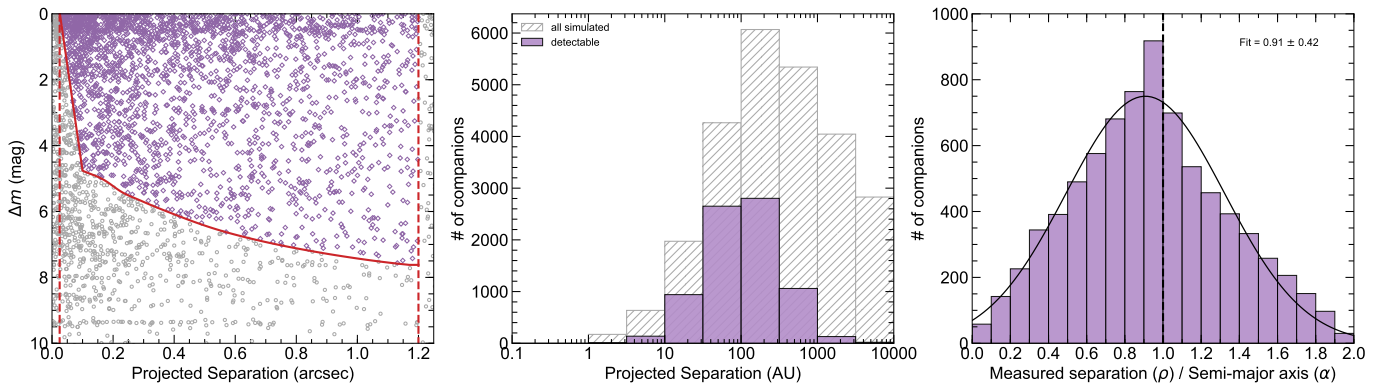
Figure 8. Same as Figure 6, but for simulated binaries created using the Moe & Kratter (2019) model.

normal period distributions against the distribution of companions seen by Gemini and WIYN. We found that a log-normal distribution with a peak at $\log P = 6.2$ days and width of $\sigma = 1.2$ minimized the χ^2 between the simulated and observed companion separations. The simulation results using this "longer period" model are shown in Figure 7. This distribution agrees with that found by Howell et al. (2021).

Lastly, we created simulated binaries based on the model of Moe & Kratter (2019) representing the lack of close binaries as planet hosting systems. They calculated the ratio between the number of exoplanet host binaries and the number of field binaries as a function of the binary separation. For this model, we started with the Raghavan et al. (2010) period distribution, then removed a fraction of close companions within each separation range used by Moe & Kratter (2019). Within 1 AU, all companions are removed. From $1 - 200$ AU, the survival fraction increases linearly in log-space. All companions outside 200 AU are kept. These simulation results are shown in Figure 8 and have a median period of $\log P = 6.4$ days similar to the longer period model, but include more stars at large separations (typically past 1.2" where speckle interferometry is not sensitive).

3.3. *Testing Binary Separations*

When we observe a binary at a random orbital phase, are we more likely to under-estimate or over-estimate the separation compared to the true semi-major axis? To answer this question, we compared the projected angular separation to the assigned semi-major axis for all detectable companions. The right panels of Figure 6-8 show a histogram of the ratio between these two parameters (ρ/α). We then fit a Gaussian to this distribution and found that the mean ratio is 0.97 ± 0.41 for the Raghavan et al. (2010) model, 0.90 ± 0.42 for the longer period model, and 0.91 ± 0.42 for the Moe & Kratter (2019) model. These ratio distributions are statistically consistent based on p-values of 0.05 found from comparing each distribution to the others using a Kolmogorov-Smirnov test. Therefore, our observed separation distribution is only slightly underestimated, and the projected separation measured in one observation is likely a reasonable estimate until the true semi-major axis can be found by resolving the full visual orbit.

4. RESULTS

4.1. *Binary Exoplanet Host Orbital Period Distribution*

Figure 9 shows the logarithmic separation distribution for the 65 companions of Solar-type exoplanet hosts found by speckle imaging at Gemini (this work) and

WIYN (Howell et al. 2021), compared to the predictions of three different binary period distributions. All predictions use a companion frequency of 46%. The observed companions peak at larger separations ($\sim$100 AU) than predicted by the field binary model (50 AU, Raghavan et al. 2010). The field binary model has a reduced χ^2 value of 4.5 and predicted a total of 56 companions, indicating that this period distribution is also too wide. Next, the "longer period model" ($\log P = 6.2$ days, $\sigma = 1.2$) is based on the observed distribution, so naturally peaks at larger separations. This model has the lowest reduced χ^2 value of 1.1 and predicts 67 companions. Lastly, the Moe & Kratter (2019) model matches the observed distribution well with a reduced χ^2 value of 1.3. It also best matches the total number of companions by predicting 65 would be detected. Overall, both the longer period model and the Moe & Kratter (2019) model provide good fits to the observed companion distribution, but we can not statistically distinguish between the two. Future work to include common proper motion binaries from Gaia could help differentiate between these models at larger orbital separations (e.g., Ziegler et al. 2021). Lastly, excluding the APC systems from our sample would remove up to two companions from each histogram bin, but the overall shape would remain intact. The observed companions would still peak at 100 AU, supporting our conclusion that binary exoplanet hosts have larger separations than field binaries.

4.2. *Exoplanet Candidate Properties*

We investigated if any correlations existed between the exoplanet candidate properties (such as radius or orbital period), the presence of a stellar companion, and the orbital properties of that companion. The planet parameters were taken from ExoFOP[3], and the radii of planets in binary systems have been corrected for "third-light" contamination from the companion star that dilutes the transits (Ciardi et al. 2015). Table 2 lists the radius correction factor, apparent radius from Exo-FOP (when available), and the corrected radius for each planet found in a binary system with $\rho < 1.2$", assuming the planet orbits the brighter, primary component. Our sample includes some planet candidates with radii larger than $20 R_\oplus$, which are likely red dwarf companions.

The left panel of Figure 10 shows the planet radius as a function of the planet's period, color coded by whether the host star is single or part of a binary system. Gi-

---

[3] The planet radii were estimated using the stellar radii from the TESS Input Catalog, which does not account for the multiplicity of the host stars and therefore could underestimate the radii of stars with bright, unresolved companions.
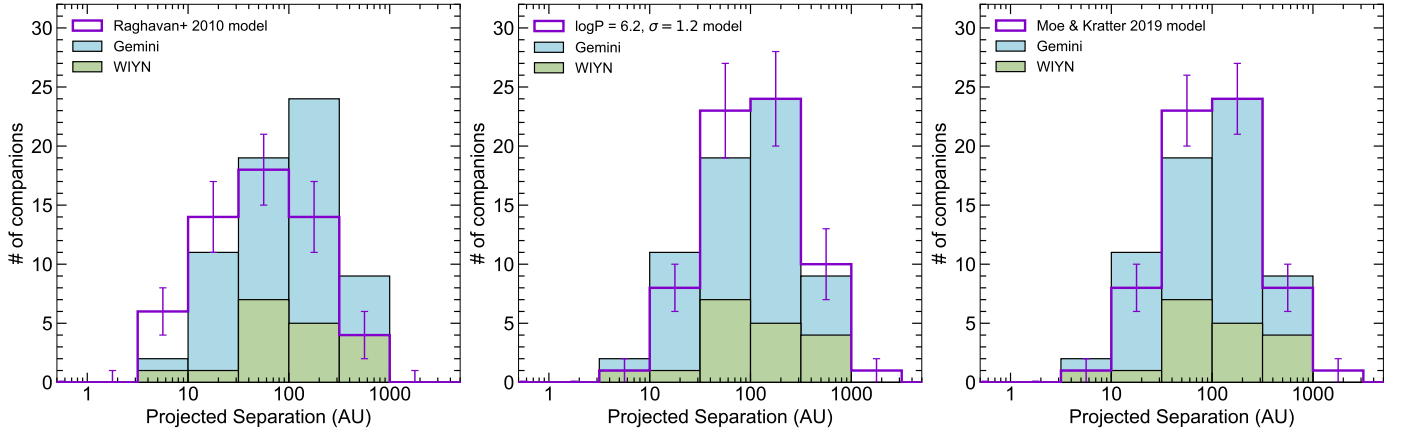
Figure 9. Histograms for the projected physical separation in logarithmic bins. The solid bars correspond to the companions with separations less than 1.2" around solar-type exoplanet host stars detected by Gemini (blue) and WIYN (Howell et al. 2021, green). The purple unfilled histograms correspond to the expected number of companions based on the field binary period distribution (left), on a distribution peaking at longer periods (middle), and on the Moe & Kratter (2019) model (right).
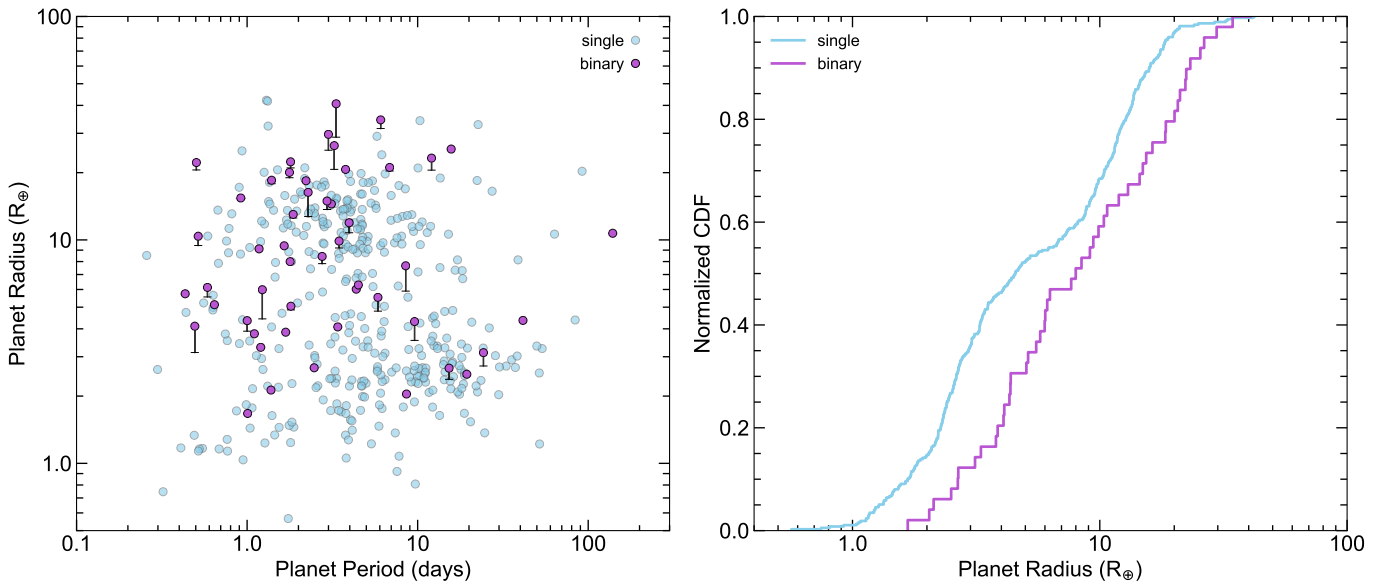
Figure 10. *Left:* Planet radius as a function of orbital period for planet candidate hosts in single star systems (light blue) and in close binary systems (purple). For the planets in binaries, we show the increase in radius (tail to plotted point) when correcting for dilution by the companion. *Right:* Normalized cumulative distribution function for the radii of planets in single and binary systems. The two subsamples appear similar, except for the clear observational bias against detecting Earth-sized, transiting planets in binary systems.

ant planet candidates are seen at all periods independant of host binarity. However, we see an observational bias against the detection of Earth-sized ($R_{pl} < 2\ R_\oplus$), transiting planet candidates in binary star systems. Using the Kolmogorov-Smirnov test to compare the radius distribution of planets in binaries to those around single stars, we found a p-value of 0.001 indicating that these subsamples are statistically different. This is also evident in the right panel of Figure 10 that shows the cumulative distribution function for these two subsamples and the lack of Earth-sized, transiting planets in binary systems. Savel et al. (2020) investigated this observational bias and found that the occurence rates for super-Earths and sub-Neptunes are underestimated by roughly 26% if transit dilution from stellar companions is not taken into account. In addition, this effect will manifest itself more strongly as the planet orbital period becomes longer (fewer measured transits, lower signal-to-noise ratio) making planets approaching or in the Habitable Zone particularly susceptible to this bias.

Figure 11 shows the separations of the planet candidates and stellar companions for the 58 host binaries in

our sample with $\rho < 1.2$" and sorted by companion separation. No corresponding trend with the planet separation is seen, likely because the companions are at least $100\times$ farther from the host stars than the planets and well beyond the limit for dynamically stable circumstellar systems (roughly $5-10\times$, Holman & Wiegert 1999). However, TESS cannot detect longer period planets due to its short observation window, so revisits to these systems during the extended mission will be highly valuable to search for longer period planets and investigate whether their separations are influenced by the stellar companions.

5. CONCLUSIONS

We observed 517 TOI stars using speckle interferometry at Gemini in search of stellar companions to validate and characterize the exoplanets and their stellar environments. We detected 73 companions around exoplanet candidate host TOI's and 29 companions around false positive TOI's and present the binary parameters for each system. The magnitude differences of exoplanet host binaries can be used to correct for transit dilution when calculating the exoplanet radii and density (Ciardi et al. 2015), but additional observations may be needed to determine around which stellar component the planet is actually orbiting (e.g., Howell et al. 2019).

We then combined our sample of exoplanet host binaries with those found with speckle interferometry at WIYN (Howell et al. 2021) in order to test the predictions of several different binary period distributions. Our results are consistent with past studies (Kraus et al. 2016; Fontanive et al. 2019; Ziegler et al. 2020, 2021; Howell et al. 2021) in showing that the binary exoplanet host period distribution is narrower and peaks at a larger value than that of field binaries, but our lack of very close companions (< 100 AU) is less dramatic than found by these previous studies due to our improved angular resolution and sensitivity to faint companions. Furthermore, our sample clearly shows the observational bias against detecting small planets in transit surveys like TESS due to the third light from a stellar companion. Both the host star multiplicity and this observational bias must be taken into account when calculating the occurence rates of Earth-sized planets (Ciardi et al. 2015; Furlan et al. 2017; Savel et al. 2020). We did not find any additional correlations in the properties of the planets or companions in our sample.

Finally, understanding how binary companions affect the formation, evolution, and survival of exoplanets is an important component to understanding planet formation overall. This work focused on the impact of the binary separation, but the relative inclination between the planet and companion, the eccentricity of the binary orbit, and the mass ratio are other important factors (e.g., Holman & Wiegert 1999; Quintana et al. 2002; Jang-Condell 2015). We are currently monitoring exoplanet host binaries with shorter periods to resolve the visual and spectroscopic orbits and determine each system's orbital parameters (e.g., Colton et al. 2021). We plan to test each system's dynamical stability and potential for habitable planets in order to investigate how these other binary properties affect planet formation and survival.

Figure 11. Planet and stellar companion separations for the binary exoplanet host systems observed with Gemini. The planets are plotted as red circles (size scaled with the cube root of the planet radius) and the stellar companions are plotted as blue circles (size scaled with the binary mass ratio). The systems are sorted by the stellar companion separation. We see no obvious trends between the two populations, perhaps not unexpected for the very short orbital period planet detections common for TESS.

Table 2. Corrected Radii of Planet Candidates in Close Binary Systems

Planet Candidate	Correction Factor	Apparent R_{pl} ($R_\oplus$)	Corrected R_{pl} ($R_\oplus$)	Planet Candidate	Correction Factor	Apparent R_{pl} ($R_\oplus$)	Corrected R_{pl} ($R_\oplus$)
TOI 140.01	1.282	12.74	16.33	TOI 1037.01	1.005	3.29	3.31
TOI 141.01	1.007	1.66	1.67	TOI 1039.01	1.053	$\cdots$	$\cdots$
TOI 224.01	1.182	14.75	17.44	TOI 1131.01	1.103	5.56	6.13
TOI 235.01	1.119	$\cdots$	$\cdots$	TOI 1133.01	1.038	4.86	5.05
TOI 252.01	1.114	3.90	4.35	TOI 1189.01	1.109	10.76	11.93
TOI 264.01	1.008	18.25	18.40	TOI 1191.01	1.005	25.36	25.50
TOI 271.01	1.005	2.66	2.68	TOI 1192.01	1.034	11.65	12.04
TOI 287.01	1.013	20.41	20.68	TOI 1204.01	1.005	2.12	2.13
TOI 291.01	1.132	20.52	23.23	TOI 1217.01	1.005	4.34	4.36
TOI 309.01	1.178	$\cdots$	$\cdots$	TOI 1293.01*	1.000	3.86	3.86
TOI 325.01	1.012	5.95	6.02	TOI 1335.01	1.411	28.83	40.67
TOI 354.01	1.178	25.20	29.68	TOI 1343.01	1.004	4.06	4.08
TOI 364.01	1.312	3.13	4.11	TOI 1447.01	1.351	4.43	5.99
TOI 380.01	1.079	20.57	22.19	TOI 1491.01	1.008	6.24	6.29
TOI 457.01*	1.000	9.12	9.12	TOI 1531.01	1.100	9.44	10.38
TOI 487.01	1.147	2.73	3.13	TOI 1544.01	1.018	$\cdots$	$\cdots$
TOI 487.02	1.147	$\cdots$	$\cdots$	TOI 1559.01	1.074	9.20	9.88
TOI 492.01	1.014	14.29	14.49	TOI 1565.01	1.212	23.87	28.93
TOI 564.01	1.005	9.36	9.41	TOI 1598.01	1.006	3.78	3.80
TOI 568.01	1.214	3.55	4.31	TOI 1636.01	1.056	18.98	20.05
TOI 680.01	$\cdots$	5.74	$\cdots$	TOI 1641.01	1.037	12.54	13.00
TOI 697.01	1.004	2.03	2.04	TOI 1677.01	1.008	5.09	5.13
TOI 722.01	1.122	2.38	2.67	TOI 1678.01	1.037	20.34	21.10
TOI 791.01	1.003	10.68	10.71	TOI 1719.01	1.077	7.83	8.43
TOI 798.01	1.321	$\cdots$	$\cdots$	TOI 1740.01	1.018	2.46	2.51
TOI 854.01	1.152	4.80	5.53	TOI 2035.01	1.298	5.90	7.66
TOI 926.01	1.065	21.00	22.37	TOI 2220.01	1.036	17.85	18.49
TOI 931.01	1.277	20.69	26.42	TOI 2305.01	1.013	15.21	15.40
TOI 952.01	1.019	7.84	7.99	TOI 2310.01	1.091	13.68	14.93
TOI 1035.01	1.094	31.50	34.45				

*The companion for this TOI is listed as a nearby star in ExoFOP, so its flux has already been accounted for when calculating the planet radius.

APPENDIX

Our Gemini North & South observations are listed in Tables 3 and 4, respectively. Each observing log contains the TOI number, TESS magnitude, the inverse of the parallax from Gaia EDR3 (Gaia Collaboration et al. 2016, 2020) for the distance, effective temperature from the TESS Input Catalog (Stassun et al. 2019), UT date of observation, the 5σ contrast limits at $0.2''$ and $1.0''$ in the blue and red filters, and notes for each target. The Julian date of each observation can be found in the headers of the archival data hosted on the Gemini Observatory Archive. If a star's distance was not available in Gaia EDR3, then the value from DR2 or ExoFOP was used. Examples of target notes include false positive identifications and other names of the host star with confirmed exoplanets.

Table 3. Gemini North Observing Log

TOI	TIC	TESS Mag.	Distance (pc)	$T_{\rm eff}$ (K)	UT Date (MM/DD/YY)	ΔMag (562 nm) $0.2''$	$1.0''$	ΔMag (832 nm) $0.2''$	$1.0''$	Notes
139	62483237	9.4	42.4	4356	10/12/19	4.00	4.45	5.02	7.35	
143	25375553	9.8	288.4	6371	6/9/19	4.48	5.30	5.30	8.74	WASP-111
162	99493790	11.7	275.1	5405	6/9/19	3.70	3.91	5.07	7.32	APC
198	12421862	9.9	23.8	3763	10/9/19	3.77	4.31	5.46	8.19	
					8/4/20	4.06	4.40	5.31	7.60	
223	326453034	10.3	369.7	5063	10/12/19	4.14	4.38	5.40	7.54	
225	47525799	11.0	115.8	4658	10/13/19	3.77	4.01	5.09	7.72	
227	2760710	13.8	52.6	2808	10/13/19	4.06	4.21	4.90	6.32	
230	160074939	8.7	141.6	6467	10/15/19	3.66	3.68	5.32	5.85	False alarm
233	415969908	11.3	33.7	3644	10/14/19	4.01	4.25	5.28	7.49	
234	12423815	14.6	253.5	3642	10/15/19	4.00	4.05	4.75	4.94	
238	9006668	9.9	80.2	5024	10/12/19	4.33	4.69	5.50	8.32	
244	118327550	10.3	22.1	3342	10/14/19	4.18	4.40	5.01	6.41	
					8/4/20	3.90	4.14	5.35	6.61	
245	154618248	8.4	123.0	6208	10/15/19	4.27	4.48	5.34	7.11	
256	92226327	11.3	319.2	3131	8/10/20	4.16	4.56	5.08	8.10	LHS 1140
260	37749396	8.5	20.2	4111	10/12/19	4.88	5.16	5.23	8.08	
261	63898957	9.0	113.6	5890	10/13/19	4.32	4.79	5.40	7.77	
262	70513361	8.1	44.1	5302	10/15/19	4.10	4.61	5.36	7.91	
263	120916706	15.6	286.9	3116	10/15/19	3.75	3.88	4.76	4.96	
266	164767175	9.5	101.7	5784	10/15/19	4.47	4.70	5.14	7.81	
277	439456714	11.7	64.9	3748	8/10/20	4.11	4.54	5.47	7.48	
278	244161191	13.2	44.8	2955	10/12/19	3.97	4.29	4.56	4.81	
280	42054565	10.0	99.6	5454	10/14/19	3.54	3.72	5.13	6.88	
287	2758565	12.4	523.3	5807	10/12/19	4.28	4.35	5.05	5.98	
288	47316976	9.0	211.3	6530	10/13/19	4.13	4.52	5.18	7.60	
292	180285396	13.3	297.6	4463	10/15/19	3.41	3.52	4.52	5.30	
294	188570092	11.4	126.8	4521	10/12/19	4.21	4.54	5.10	7.81	HATS-72
298	206686292	12.8	971.4	6273	10/15/19	3.81	4.10	4.43	5.61	APC
307	9100874	13.1	745.7	5747	10/14/19	4.10	4.27	4.81	5.92	
309	228507250	12.3	481.4	5329	10/9/19	3.86	4.36	4.59	6.66	
310	175477257	12.4	545.8	5798	10/15/19	3.67	3.70	4.59	5.72	
315	66356824	12.4	546.1	5671	10/13/19	3.64	4.03	4.57	5.42	False positive

Table 3 *continued*

Table 3 *(continued)*

TOI	TIC	TESS Mag.	Distance (pc)	T_{eff} (K)	UT Date (MM/DD/YY)	ΔMag (562 nm) 0.2″	1.0″	ΔMag (832 nm) 0.2″	1.0″	Notes
323	251852984	13.4	316.3	4558	10/14/19	4.00	4.37	4.71	5.56	
325	66413476	12.0	182.4	4391	10/13/19	4.05	4.23	4.82	6.63	
327	206669860	13.5	977.3	5960	10/15/19	3.54	3.53	4.63	5.13	
329	169765334	10.7	285.6	5561	10/13/19	3.91	4.24	5.42	8.01	
330	27966179	12.9	201.2	4314	10/12/19	3.76	4.02	4.99	5.74	
341	33911302	13.3	418.9	4775	10/14/19	4.19	4.24	4.49	6.14	
343	66497310	12.4	523.9	5885	10/12/19	4.22	4.45	4.93	6.02	
344	13023378	11.9	403.5	6149	10/13/19	3.87	4.26	4.72	7.34	
355	183593642	11.0	343.5	6049	10/13/19	3.69	3.92	4.89	6.23	
360	13023738	12.3	631.2	5657	10/13/19	3.72	4.07	5.15	6.62	
364	47425697	10.5	265.7	6220	10/13/19	3.95	4.16	4.78	6.70	
366	251878904	13.5	861.0	5504	10/14/19	3.67	3.83	4.58	5.47	
370	251855940	13.5	762.6	5805	10/14/19	3.81	3.90	4.59	5.21	
378	20892672	13.1	2316.4	5894	10/9/19	4.04	4.23	4.10	5.37	False positive
390	250386181	9.9	169.4	6321	10/12/19	4.39	5.19	5.23	7.84	False positive
393	29960109	11.2	37.7	3450	10/13/19	4.12	4.35	4.92	8.59	False positive
394	9858404	8.0	141.7	6216	10/14/19	5.66	6.67	5.34	7.83	False positive
402	120896927	8.3	44.9	5175	10/15/19	4.18	4.97	5.25	7.96	
421	94986319	9.3	75.0	5718	10/9/19	4.75	5.26	5.33	9.06	
422	117979455	9.0	124.1	5999	10/9/19	4.49	5.00	5.33	8.36	
424	117979694	10.5	103.7	5059	10/9/19	4.38	4.75	5.13	7.96	False positive
426	189013224	9.6	112.8	5731	10/12/19	4.64	4.99	5.59	8.26	
427	70914192	10.4	149.1	5272	10/15/19	4.23	4.56	5.19	7.22	False positive
428	117979850	7.8	123.6	5800	10/9/19	4.71	5.33	5.36	8.66	APC
431	31374837	8.2	32.6	4891	10/15/19	4.19	4.50	5.27	7.72	
432	38686737	12.6	725.6	6846	10/14/19	4.77	5.42	5.00	6.52	False positive
433	188989177	9.1	521.5	8242	10/12/19	4.89	5.33	5.56	8.16	False positive
438	468880077	9.4	72.3	5211	12/7/20	5.48	7.05	4.97	8.26	
444	179034327	9.1	57.5	5229	10/15/19	4.26	4.51	5.06	7.54	
455	98796344	8.8	6.9	3562	10/13/19	3.96	4.60	4.83	8.58	LTT 1445 A
					12/6/20	4.38	4.66	5.57	7.94	
457	89256802	13.7	125.8	3054	10/14/19	3.97	4.22	4.64	5.28	
458	64071894	9.6	76.7	5164	10/12/19	4.42	4.83	5.32	7.94	
460	9804616	14.1	181.7	3274	10/9/19	4.23	4.42	4.66	6.30	False positive
461	4646810	8.9	45.7	4884	10/15/19	4.83	5.18	5.29	8.17	
463	176831592	9.1	184.2	6498	10/14/19	4.11	4.20	5.43	6.78	False positive
464	398733009	15.6	3544.9	31000	10/13/19	3.94	3.98	4.41	4.83	False positive
492	17746821	11.3	490.6	6280	12/5/20	5.15	5.53	5.51	6.37	HAT-P-50
511	440777904	11.3	413.2	6373	12/5/20	5.05	6.06	4.96	6.94	HAT-P-24
514	366576758	13.7	479.4	5027	12/5/20	4.82	4.99	4.22	5.11	K2-114
515	366622912	13.8	447.4	4973	2/15/20	4.74	5.16	4.62	5.82	
519	218795833	14.4	115.2	3225	2/18/20	3.90	3.98	4.73	5.00	
521	27649847	12.4	61.0	3439	2/18/20	4.64	4.89	5.19	6.41	
526	200593988	12.3	70.9	3617	12/5/20	4.83	5.15	5.10	6.35	
530	387690507	13.5	147.7	3688	2/17/20	4.73	4.96	4.84	5.59	
532	144700903	12.7	135.3	3946	12/5/20	4.88	5.21	5.24	6.23	

Table 3 *continued*

Table 3 *(continued)*

TOI	TIC	TESS Mag.	Distance (pc)	$T_{\rm eff}$ (K)	UT Date (MM/DD/YY)	ΔMag (562 nm) 0.2″	1.0″	ΔMag (832 nm) 0.2″	1.0″	Notes
534	281909674	14.4	1255.5	5945	12/7/20	4.62	4.99	4.93	5.48	CoRoT-13
535	280210963	14.8	1144.1	5675	12/7/20	4.53	4.83	5.44	6.25	CoRoT-12
547	36352297	13.1	769.2	5950	12/7/20	4.64	5.17	5.32	6.72	CoRoT-1
552	44737596	13.8	197.6	3654	10/14/19	4.16	4.18	4.73	5.62	
554	407966340	6.4	45.2	6338	2/15/20	5.46	7.25	5.45	9.02	
557	55488511	11.6	75.5	3883	10/13/19	4.08	4.31	5.32	7.83	
559	209459275	10.6	232.9	5972	10/9/19	3.86	4.35	5.03	7.38	
562	413248763	8.7	9.4	3505	2/16/20	4.23	4.58	5.08	7.56	GJ 357
564	1003831	10.7	198.8	5752	2/18/20	4.35	4.45	5.06	6.90	
571	270468559	11.6	413.9	5743	12/5/20	4.86	5.13	5.31	6.30	HAT-P-42
573	296780789	12.5	88.7	3404	2/15/20	4.24	4.67	5.03	6.37	TIC 876200724
576	408310006	8.9	114.3	6313	12/7/20	4.76	5.63	4.89	8.46	WASP-166
626	65412605	9.5	426.8	8490	10/15/19	4.12	4.33	5.21	7.44	False positive
631	97158538	8.8	229.1	6852	10/15/19	4.01	4.28	5.28	7.54	False positive
635	286132427	8.1	59.0	5914	12/7/20	5.30	6.45	4.83	7.96	False positive
649	35582553	10.0	429.2	6779	12/6/20	4.50	4.88	5.08	7.40	
651	72090501	6.8	80.3	8577	12/6/20	4.58	5.39	5.49	8.63	
652	22221375	7.4	45.6	5903	12/7/20	5.27	6.06	5.41	8.82	
654	35009898	12.2	57.8	3433	6/9/19	4.27	4.38	5.24	7.10	
					2/15/20	4.29	4.65	5.35	7.61	
656	36734222	11.1	87.2	4400	6/9/19	4.08	4.47	5.23	7.61	WASP-43
658	48476907	9.5	281.1	6521	2/17/20	4.09	4.25	4.98	6.54	
659	48476908	10.2	245.3	5990	2/17/20	4.15	4.23	4.74	6.42	
660	53189332	11.0	359.3	6055	6/9/19	4.21	4.69	5.17	7.21	WASP-106
663	54962195	11.8	63.9	3719	6/10/19	3.89	4.62	5.00	7.61	
664	55092869	7.3	100.0	5370	6/9/19	4.79	5.53	4.97	7.81	KELT-11
669	124573851	10.2	142.5	5582	2/15/20	4.98	5.56	5.45	8.38	
675	169226822	9.6	160.7	5620	6/9/19	4.32	4.95	5.25	8.03	WASP-127
676	219187649	13.5	709.3	5430	2/16/20	4.44	4.64	4.47	5.10	
679	308050066	10.0	309.1	6655	6/10/19	4.10	4.71	5.19	8.32	False positive
680	335499997	9.0	160.1	5967	2/18/20	4.81	5.67	5.28	7.83	APC
692	320417762	9.0	483.0	9622	12/5/20	6.09	6.99	5.29	7.22	
697	77253676	9.4	92.9	5447	10/15/19	3.63	3.80	5.08	7.00	
727	149788158	11.0	42.7	3653	2/18/20	4.18	4.33	5.52	7.03	
728	96097215	10.3	172.2	5648	2/16/20	4.80	5.13	4.97	7.13	
729	144138509	10.6	243.5	6023	2/18/20	4.70	5.26	5.49	7.38	
732	36724087	10.6	22.0	3329	2/18/20	4.66	4.95	5.42	7.02	LTT 3780
736	181804752	13.6	26.7	2940	6/8/19	3.78	4.03	5.19	6.97	LP 791-18
737	219189765	14.8	292.0	3394	2/16/20	4.14	4.23	4.16	4.93	
821	125405602	11.2	39.7	3669	2/16/20	4.64	4.92	4.78	6.40	False alarm
836	440887364	8.6	27.5	4476	2/16/20	4.58	4.94	5.08	6.96	
844	380886535	11.8	493.5	5830	12/7/20	4.66	5.04	5.25	6.74	False positive
849	33595516	11.5	225.5	5311	10/15/19	3.79	4.09	4.72	6.24	
850	423670610	11.3	357.3	5864	10/15/19	4.13	4.10	4.90	6.76	APC
851	40083958	11.0	169.6	5485	10/13/19	4.39	5.03	4.73	7.45	
852	29918916	10.9	358.5	5574	10/9/19	4.34	4.75	5.18	8.18	

Table 3 *continued*

Table 3 *(continued)*

TOI	TIC	TESS Mag.	Distance (pc)	$T_{\rm eff}$ (K)	UT Date (MM/DD/YY)	ΔMag (562 nm) 0.2″	1.0″	ΔMag (832 nm) 0.2″	1.0″	Notes
857	404467699	10.3	288.3	6143	8/10/20	4.63	5.31	5.71	8.35	WASP-137
865	44797824	9.8	136.6	5181	10/14/19	4.30	4.59	5.24	7.91	APC
880	34077285	9.3	60.6	4935	10/15/19	4.38	4.75	5.25	7.48	
883	123846039	9.4	102.5	5651	12/7/20	5.03	5.96	5.40	9.04	
884	167031605	10.0	1012.8	11246	2/15/20	5.50	7.16	5.24	8.48	False positive
892	66561343	11.0	334.9	7723	10/14/19	4.38	4.75	5.23	7.62	
893	123958679	11.5	1319.0	9856	12/7/20	4.72	5.34	5.31	7.70	
894	42755801	9.2	359.5	9900	10/15/19	4.71	5.18	5.43	6.68	False positive
895	250484865	8.8	95.7	5998	2/18/20	4.99	5.74	5.21	7.99	False positive
898	124543547	10.6	479.5	5652	10/12/19	4.39	4.77	5.00	7.03	False positive
938	332660150	10.8	213.1	5981	10/15/19	4.27	4.44	4.98	6.72	
939	67772767	10.9	349.3	6160	10/9/19	4.55	5.01	5.29	7.68	
942	146520535	11.0	151.4	4945	10/14/19	4.30	4.69	5.00	7.74	
952	319312479	10.1	417.1	7110	10/13/19	4.48	4.97	5.12	7.60	
954	44792534	9.8	239.1	5756	10/14/19	4.41	4.69	5.38	7.98	
955	146467675	9.7	208.2	5889	10/14/19	4.41	4.63	5.41	8.01	False positive
958	92880568	11.0	292.8	5745	10/9/19	4.15	4.57	5.33	7.71	APC
960	5109298	10.7	719.0	9385	12/7/20	4.83	5.50	5.53	7.78	False positive
982	177126182	10.3	713.3	8502	12/7/20	4.67	5.33	5.21	7.66	False positive
991	7561203	10.1	621.8	9855	12/6/20	4.65	5.17	5.35	7.65	
993	259353953	10.1	353.4	8035	12/6/20	4.27	4.50	5.43	7.96	
1000	50365310	9.6	513.8	10249	12/6/20	4.78	5.51	5.53	7.91	False positive
1007	65212867	8.9	271.8	6596	12/6/20	5.29	6.14	5.21	8.44	
1022	47384844	8.7	118.4	6084	2/15/20	4.96	5.52	5.52	8.25	
1027	20318757	10.2	56.5	4272	2/16/20	4.11	4.27	5.24	6.76	
1049	16288184	11.1	307.3	6599	6/8/19	3.75	3.99	5.09	6.65	K2-237 (EPIC 229426032)
1131	198213332	9.3	247.6	5579	2/17/20	4.14	4.49	5.18	7.44	
1133	69997672	9.1	262.5	6244	10/12/19	5.32	6.56	5.42	8.02	
1136	142276270	8.9	84.6	5729	2/15/20	4.26	4.62	5.24	7.39	
1137	89389197	8.9	415.4	4920	10/12/19	5.04	5.81	5.47	8.31	
1139	202563254	8.9	241.7	7947	10/13/19	5.31	5.97	5.13	8.44	
1145	350995812	8.5	465.5	8563	10/12/19	5.15	6.90	5.41	8.33	
1147	288391628	8.4	206.5	6259	6/7/20	3.06	3.28	5.41	7.53	False positive
1152	237184773	7.4	104.3	5485	8/10/20	5.67	6.89	5.20	6.74	TIC 1715469662
1155	161450762	9.7	3683.2	3282	10/13/19	4.71	5.10	4.77	6.21	False positive
1160	89510024	9.6	5701.0	4000	10/12/19	4.36	4.62	4.93	6.47	
1170	294176967	10.3	906.0	7875	10/12/19	4.19	4.57	5.52	7.91	False positive
1171	101929303	10.3	488.7	7266	10/12/19	5.00	5.52	5.56	7.94	False positive
1174	154089169	10.3	94.7	5030	2/17/20	4.13	4.41	5.44	7.20	
1179	148914726	10.1	86.3	4928	2/15/20	4.00	4.54	5.34	7.61	False positive
1181	229510866	10.1	310.6	6122	8/4/20	4.04	4.45	5.34	8.06	
1185	83210867	9.9	247.5	5997	10/12/19	5.19	6.27	5.46	8.07	False positive
1189	112026224	9.9	278.1	5287	10/12/19	5.04	5.57	5.23	6.73	
1191	237185205	9.8	354.7	6800	8/10/20	5.28	7.38	5.12	8.92	
1192	158276040	10.5	375.1	6479	6/6/20	4.82	5.29	5.29	7.39	
1193	89643259	10.5	865.5	7167	10/13/19	4.49	5.01	4.97	7.11	False positive

Table 3 *continued*

Table 3 *(continued)*

TOI	TIC	TESS Mag.	Distance (pc)	$T_{\rm eff}$ (K)	UT Date (MM/DD/YY)	ΔMag (562 nm) 0.2″	1.0″	ΔMag (832 nm) 0.2″	1.0″	Notes
1194	147950620	10.5	149.2	5340	2/17/20	4.12	4.23	5.04	6.05	
1199	99869022	10.4	247.5	5618	2/17/20	4.03	4.36	5.26	6.67	
1201	29960110	10.9	37.6	3948	10/13/19	4.14	4.54	4.30	7.74	
1235	103633434	9.9	39.6	3912	2/16/20	4.08	4.26	4.91	6.81	
1238	153951307	11.3	70.6	3853	2/17/20	4.13	4.38	5.08	6.39	
1241	159107668	11.2	573.5	5826	6/7/20	4.38	4.78	4.76	6.27	KOI-5
1247	232540264	8.5	73.4	5712	2/17/20	4.26	4.59	5.35	7.53	
1248	232612416	11.1	169.9	5227	8/4/20	3.87	4.33	5.21	7.40	
1249	232976128	10.2	139.7	5453	2/17/20	3.86	4.13	5.16	7.30	
1253	233684822	9.9	185.8	5779	8/4/20	4.06	4.61	5.08	7.73	
1260	355867695	10.8	73.4	4225	2/16/20	4.16	4.27	5.02	6.68	
1261	356311210	10.7	199.9	5897	8/10/20	4.14	4.84	5.30	7.74	
1262	365938305	9.6	93.1	5396	2/17/20	4.05	4.27	5.18	6.89	
1266	467179528	11.0	36.0	3618	2/18/20	4.20	4.46	5.14	6.56	
1273	445859771	10.4	176.7	5736	2/15/20	4.45	4.90	5.28	7.46	
1277	153949511	9.8	101.0	5544	2/17/20	3.84	4.08	4.66	6.32	False alarm
1279	224297258	10.0	106.9	5477	2/15/20	4.36	5.05	5.35	8.06	
1293	202504234	10.9	236.6	5923	2/17/20	3.76	3.80	5.30	7.06	
1294	219015370	10.9	331.7	5714	2/17/20	4.09	4.29	5.29	6.57	
1300	293687315	9.8	316.4	6840	8/4/20	4.15	4.74	5.11	7.69	KELT-18
1301	356867115	10.5	91.2	4820	6/6/20	4.08	4.22	5.13	6.83	
1335	89759617	10.5	694.8	7965	8/4/20	4.95	6.19	4.76	7.34	
1336	92783821	10.2	521.0	7396	8/4/20	5.42	6.95	5.34	8.33	
1339	269701147	8.3	53.5	5556	6/6/20	4.06	5.02	5.45	8.05	HD 191939
1343	358631536	10.0	396.3	9622	8/10/20	5.07	5.98	4.99	7.74	
1345	160487753	10.8	757.7	5146	2/16/20	4.43	4.78	4.45	6.06	
1353	279177746	10.2	450.4	9706	6/6/20	5.32	6.10	5.63	8.02	
1373	176899385	10.0	274.3	6893	8/10/20	5.43	6.71	5.45	8.21	HAT-P-6
					12/6/20	5.02	5.64	5.44	7.78	
1378	249812036	9.6	573.8	8224	8/10/20	5.28	6.25	5.59	8.12	APC
1410	199444169	10.2	72.6	4635	8/10/20	4.93	5.74	5.50	8.54	
1411	116483514	9.1	32.5	4184	6/7/20	4.84	5.88	5.33	8.50	
1412	116483734	11.1	79.2	4223	6/7/20	4.67	5.39	5.13	8.14	APC
1413	119700084	10.1	121.0	5427	12/3/20	5.25	5.57	5.21	7.08	
1415	148782377	8.4	112.0	6383	6/7/20	5.36	6.49	5.30	8.26	
1416	158025009	9.1	55.0	4946	6/7/20	5.27	6.06	5.53	8.39	
1417	164173105	8.5	153.4	7164	12/3/20	5.56	6.50	5.22	7.40	False positive
1418	224600500	6.8	159.3	8475	2/18/20	4.33	5.35	5.22	8.16	False positive
1424	418959198	10.5	87.7	4529	12/2/20	5.27	6.56	5.37	8.03	
1434	138588540	8.1	37.8	5394	2/17/20	3.78	4.49	5.05	7.76	
1435	153976959	10.0	93.1	5142	2/18/20	3.66	3.83	5.28	7.22	
					6/7/20	4.03	4.47	5.54	7.75	
1436	154383539	11.1	131.2	5011	2/15/20	4.50	4.79	4.99	7.19	
1437	198356533	8.7	103.4	6093	2/18/20	4.26	4.68	5.45	7.48	
1440	233617847	9.6	236.5	5780	8/4/20	3.75	4.56	5.16	7.52	
1442	235683377	12.5	41.4	3328	6/7/20	3.90	4.06	5.03	6.12	

Table 3 *continued*

Table 3 *(continued)*

TOI	TIC	TESS Mag.	Distance (pc)	T_{eff} (K)	UT Date (MM/DD/YY)	ΔMag (562 nm) 0.2″	1.0″	ΔMag (832 nm) 0.2″	1.0″	Notes
1447	298073824	8.1	310.7	6906	2/15/20	3.81	4.24	5.20	6.61	
1451	417931607	9.0	90.8	5781	2/15/20	4.12	4.77	5.31	8.07	
1467	240968774	10.6	37.5	3834	8/9/20	4.66	5.13	5.33	7.16	
					12/4/20	4.66	5.24	5.25	7.76	
1468	243185500	10.9	24.7	3382	8/4/20	4.92	5.38	5.07	7.02	
1471	306263608	8.6	67.3	5626	12/4/20	5.76	7.94	5.51	8.40	
1472	306955329	10.6	122.0	5103	12/3/20	4.73	5.31	5.42	7.28	
1476	432549364	10.2	271.5	6596	12/6/20	4.94	6.41	5.52	7.69	KELT-1
1478	409794137	10.2	152.3	5623	2/18/20	4.31	4.53	5.44	7.06	
1487	459978312	5.3	109.7	5047	2/18/20	5.00	5.32	4.83	7.87	False alarm
1490	283474780	8.4	240.3	4939	12/3/20	5.50	7.24	4.93	7.73	
1491	53875855	10.4	208.3	5899	12/3/20	5.40	6.76	5.14	7.75	
1493	15692883	9.7	360.0	6064	12/6/20	5.55	7.37	5.64	7.86	WASP-187
1499	414870287	7.8	3239.8	3295	8/10/20	4.28	4.78	5.72	8.89	False positive
1516	376637093	10.4	246.7	6485	8/4/20	4.08	4.53	5.19	7.61	
1531	312678993	8.4	541.5	5096	12/3/20	4.74	5.57	4.56	7.53	APC
1540	318746829	10.4	2409.6	3593	8/10/20	4.11	4.47	5.46	7.88	False positive
1543	431585347	10.1	607.6	9238	12/2/20	4.66	5.28	5.37	8.13	False positive
1544	455791689	10.4	984.0	4630	8/10/20	4.93	5.67	5.68	8.18	
1546	194203348	9.9	249.2	6223	12/6/20	5.03	5.91	5.31	7.44	
1552	326919774	8.2	469.9	9146	12/6/20	5.65	6.27	5.20	7.69	
1557	320506985	10.5	289.7	5751	12/2/20	4.43	4.92	5.30	7.60	False positive
1559	241040309	10.4	696.0	8455	12/2/20	4.81	6.06	5.27	8.13	
1560	241076290	10.2	535.3	9035	12/2/20	4.54	5.34	5.29	7.75	
1563	249945230	9.4	50.8	4582	12/2/20	4.61	5.26	5.46	8.36	
1565	251384275	9.2	328.7	8494	12/3/20	3.70	4.05	4.86	7.21	No *Gaia* parallax available
1576	327011842	9.8	484.0	4975	12/6/20	4.69	5.63	4.95	7.39	
1578	348135793	10.1	347.7	6742	12/2/20	4.33	4.93	5.43	7.99	False positive
1580	354469661	9.2	228.3	6333	12/2/20	4.80	5.38	5.50	8.72	HAT-P-59
1587	458914949	10.3	511.3	7275	12/3/20	4.17	4.46	5.28	6.98	
1591	82010657	9.6	286.4	7519	12/3/20	4.08	4.43	5.36	7.20	False positive
1592	186599508	9.8	169.9	5670	2/15/20	4.61	5.08	5.41	7.69	False positive
1598	67418624	8.6	140.9	6011	12/6/20	5.33	7.18	5.04	7.91	
1601	139375960	10.1	334.9	5917	12/3/20	5.35	6.15	5.47	7.60	
1602	129991079	10.4	209.6	6176	12/3/20	5.16	6.11	5.04	7.55	
1603	73448352	10.2	282.4	6739	12/4/20	5.58	7.22	5.28	8.24	HAT-P-47
1605	101037590	9.6	159.1	5597	12/2/20	5.38	7.40	5.53	8.64	
1607	26433869	8.4	336.7	4963	2/16/20	5.57	6.05	5.14	7.35	False positive
1634	201186294	11.0	35.1	3455	2/16/20	4.49	4.94	5.19	6.64	
					12/2/20	4.75	5.66	5.38	7.91	
1636	269892793	11.9	151.6	4769	2/18/20	4.36	4.63	5.07	6.05	APC
1638	312862941	12.1	126.3	3810	12/3/20	4.61	4.77	4.75	6.41	
1639	348673213	13.0	154.1	3896	12/2/20	4.21	4.49	5.04	6.67	
1641	422923265	9.6	622.1	9898	12/3/20	5.25	6.50	5.01	7.62	
1650	122485078	10.0	443.9	7719	2/15/20	4.80	5.80	5.24	8.80	False positive
1655	266500992	10.3	163.1	5411	12/3/20	4.96	5.24	5.29	7.24	

Table 3 *continued*

Table 3 *(continued)*

TOI	TIC	TESS Mag.	Distance (pc)	$T_{\rm eff}$ (K)	UT Date (MM/DD/YY)	ΔMag (562 nm) 0.2″	1.0″	ΔMag (832 nm) 0.2″	1.0″	Notes
1658	286561122	10.3	512.3	7326	12/4/20	5.17	6.77	5.38	8.09	
1662	339538183	9.7	349.5	7235	12/3/20	4.28	4.53	5.02	6.90	False positive
1663	353367071	9.8	386.8	7896	2/18/20	5.15	6.01	5.12	7.64	False positive
1665	354006740	6.3	66.4	6482	2/15/20	5.79	7.51	5.27	9.33	False positive
1666	368536386	10.4	410.8	7185	2/15/20	4.91	5.64	5.18	8.39	False positive
1673	470315428	10.2	210.9	5563	12/3/20	4.82	5.16	5.41	6.79	False positive
1675	81831095	10.0	383.0	7478	12/3/20	3.94	4.37	5.17	7.23	
1677	87090944	10.1	223.3	5920	2/16/20	4.80	5.21	5.28	6.62	
1678	96291218	10.4	705.8	8001	2/18/20	4.92	5.34	5.25	7.48	
1681	321041369	10.4	153.6	5673	12/3/20	4.28	4.30	4.95	6.52	
1682	367366318	8.1	135.5	6768	12/2/20	5.76	8.23	5.04	9.09	KELT-7
1683	58542531	9.8	50.9	4402	12/2/20	5.48	7.50	4.97	8.71	
1693	353475866	10.7	30.8	3474	2/18/20	4.59	4.96	5.50	7.44	
1696	470381900	14.0	64.6	3181	12/3/20	5.02	5.20	4.47	4.95	
1703	453387619	10.6	198.2	5748	12/2/20	4.73	5.96	5.45	8.39	
1719	293617835	7.8	236.5	6096	12/4/20	4.84	5.61	5.04	7.83	
1727	241225337	9.8	114.6	5566	12/3/20	4.73	5.25	5.32	7.29	
1740	174041208	10.4	116.4	5366	8/10/20	5.22	6.37	5.50	8.43	
					12/6/20	5.22	6.37	5.50	8.43	
1748	233071926	10.6	101.6	4837	8/9/20	3.86	4.20	5.27	6.86	
1795	135083444	10.1	184.3	6071	6/7/20	5.22	6.90	5.31	7.49	False positive
1797	368435330	8.6	82.3	5922	6/9/20	5.32	5.99	5.71	8.42	
1808	307734817	11.7	541.9	6352	6/6/20	4.60	5.21	5.39	6.70	False positive
1819	341815767	9.0	159.8	6610	8/10/20	4.78	5.41	5.32	8.17	
1823	142381532	9.8	71.7	4760	6/8/20	3.73	3.99	4.99	6.72	
1830	20182165	7.0	50.3	6327	8/4/20	5.31	7.00	5.14	8.36	False positive
					8/10/20	5.35	6.77	5.18	8.95	
1845	272758199	12.9	422.8	5271	6/7/20	4.04	4.18	4.83	5.88	
1847	54002556	11.6	188.9	5076	8/10/20	4.34	4.67	5.37	7.51	NGTS-11
1848	219824469	10.5	297.1	5923	6/7/20	4.48	5.02	5.32	7.51	
1852	219728669	13.5	550.4	5356	6/6/20	4.80	5.50	4.93	6.33	
1859	229742722	9.9	223.5	6415	6/7/20	4.13	4.46	5.06	7.31	
1896	174302697	8.9	169.9	6750	12/2/20	4.85	5.73	4.92	8.17	
1908	37718056	11.7	540.3	6239	8/10/20	4.25	5.09	5.28	7.80	WASP-158
1935	176685457	12.3	601.9	6245	12/7/20	4.30	4.85	5.04	7.19	NGTS-9
2009	243187830	7.4	20.5	4755	12/6/20	5.79	8.15	5.11	8.56	
2010	26547036	9.3	108.4	5842	6/7/20	3.94	4.30	5.18	7.99	
2031	470127886	10.8	279.4	6664	8/4/20	3.71	4.27	4.94	6.37	
2035	53709089	9.1	359.4	9387	12/3/20	3.98	4.37	4.53	7.06	No *Gaia* parallax available
2041	54364414	10.5	176.3	5825	8/9/20	4.04	4.31	5.53	7.37	False positive
2043	346929661	10.2	201.7	6178	8/9/20	4.04	4.41	4.97	7.15	
2059	403308915	10.2	382.3	8398	12/2/20	4.48	5.00	5.27	7.92	
2062	373785851	10.2	487.6	6895	12/3/20	4.37	4.58	5.04	7.09	False positive
2082	160039081	7.8	63.7	6004	8/10/20	4.98	5.63	5.66	8.59	
2089	341815197	11.6	187.5	5274	8/10/20	4.19	4.75	5.37	7.36	
2120	389900760	12.8	32.2	3179	12/3/20	4.28	4.50	5.07	5.88	

Table 3 *continued*

Table 3 *(continued)*

TOI	TIC	TESS Mag.	Distance (pc)	T_{eff} (K)	UT Date (MM/DD/YY)	ΔMag (562 nm) 0.2″	1.0″	ΔMag (832 nm) 0.2″	1.0″	Notes
2123	105840719	9.5	86.6	5432	8/10/20	5.61	7.09	5.53	8.88	
2293	71347873	11.8	62.8	3668	12/3/20	3.92	4.16	5.37	6.12	

Table 4. Gemini South Observing Log

TOI	TIC	TESS Mag.	Distance (pc)	T_{eff} (K)	UT Date (MM/DD/YY)	ΔMag (562 nm) 0.2″	1.0″	ΔMag (832 nm) 0.2″	1.0″	Notes
101	231663901	12.4	372.0	5600	6/20/19	4.45	4.79	4.85	5.68	WASP-46
104	231670397	9.9	317.5	6036	6/20/19	4.84	5.20	5.32	7.09	WASP-73
107	92352620	9.6	210.5	6153	5/21/19	5.36	5.64	5.60	6.71	WASP-94 A
109	29344935	13.2	515.6	5346	7/16/19	4.23	5.16	4.99	6.66	HATS-14
112	388104525	11.6	302.4	5650	11/26/20	4.28	4.67	5.44	6.82	WASP-119
116	238176110	11.0	151.2	4920	7/20/19	4.11	4.43	5.24	6.57	WASP-91
130	263003176	7.4	56.9	6296	7/17/19	4.77	5.92	4.65	7.13	
134	234994474	9.2	25.2	3794	7/14/19	4.49	4.70	5.29	7.29	L 168-9
					9/12/19	4.73	5.19	5.49	7.66	
138	277683130	9.6	191.9	5722	6/20/19	4.55	5.00	5.22	6.78	False positive
139	62483237	9.4	42.4	4356	7/20/19	5.72	7.05	5.40	7.72	
140	140068425	9.8	350.2	6174	6/20/19	4.71	5.44	4.71	6.68	APC
141	403224672	7.4	47.8	5795	6/20/19	5.25	5.99	5.20	7.74	
					6/21/19	5.51	6.11	5.46	7.78	
					7/15/19	5.40	6.05	5.28	7.90	
145	265612438	11.7	453.7	5431	6/22/19	4.67	5.30	5.32	6.66	
146	355636844	10.2	499.3	5620	7/20/19	4.54	4.99	4.99	6.81	False positive
154	389525208	10.1	401.5	5911	5/21/19	5.07	5.39	5.30	6.36	False positive
155	129637892	9.0	188.0	6221	5/22/19	4.90	5.35	5.62	7.44	
162	99493790	11.7	275.1	5405	6/20/19	4.69	5.33	5.08	6.26	APC
164	79395355	11.4	343.9	5926	6/21/19	4.71	5.41	5.25	6.20	False positive
166	147203645	10.7	172.1	5254	6/20/19	5.06	5.75	5.09	7.20	
168	369457671	11.5	129.2	4802	6/22/19	4.71	5.10	4.74	5.72	
172	29857954	10.7	358.9	5802	7/16/19	4.74	6.06	5.39	8.04	
179	207141131	8.2	38.6	5058	9/12/19	5.71	6.65	5.28	7.24	
186	279741379	7.0	16.3	4629	11/29/20	5.33	5.99	5.67	8.10	
191	183532609	9.1	90.0	5600	7/19/19	5.05	6.30	4.94	7.14	WASP-8
203	259962054	12.2	24.8	3203	11/29/20	3.99	4.20	4.70	5.67	
208	314865962	10.4	148.7	5493	11/26/20	4.13	4.41	5.08	7.38	
213	234345288	9.8	54.3	4566	11/29/20	4.26	4.44	5.45	7.34	
214	167415965	8.0	38.9	5346	3/13/20	4.45	5.39	5.55	7.41	
218	32090583	13.3	52.6	3146	11/27/20	4.15	4.49	4.83	5.58	
220	150098860	9.7	90.9	5273	1/9/20	4.71	4.96	5.52	8.10	
224	70797900	11.1	69.8	3689	11/26/20	4.63	5.24	4.71	6.86	APC
226	47484268	12.4	51.0	3396	7/17/19	4.74	5.00	5.02	6.39	False positive
232	402026209	11.8	273.1	5436	9/12/19	4.93	5.34	4.88	6.40	WASP-4

Table 4 *continued*

Table 4 *(continued)*

TOI	TIC	TESS Mag.	Distance (pc)	$T_{\rm eff}$ (K)	UT Date (MM/DD/YY)	ΔMag (562 nm) 0.2″	1.0″	ΔMag (832 nm) 0.2″	1.0″	Notes
					9/28/19	4.94	5.69	5.37	7.19	
233	415969908	11.3	33.7	3644	9/12/19	4.72	5.10	5.55	6.79	
235	280095254	9.5	137.9	5454	11/29/20	4.03	4.32	5.52	6.93	
238	9006668	9.9	80.2	5024	7/15/19	5.33	6.55	5.50	8.81	
					9/12/19	5.18	6.20	5.29	7.25	
252	237924601	11.7	258.5	5071	11/29/20	4.61	4.91	5.17	6.17	APC
254	49687222	9.8	195.2	6101	7/17/19	5.26	6.17	5.72	8.52	False alarm
					9/13/19	4.82	6.05	5.18	7.37	
					10/10/19	5.26	6.82	5.41	8.55	
257	200723869	7.0	76.9	6383	9/12/19	6.14	7.29	4.97	7.31	
260	37749396	8.5	20.2	4111	9/12/19	5.21	5.77	4.88	7.58	
263	120916706	15.6	286.9	3116	1/12/20	4.71	4.98	4.42	4.69	
264	122612091	10.5	418.6	6250	11/25/20	5.49	6.51	5.54	7.23	WASP-72
271	259511357	8.4	99.9	6025	9/13/19	5.23	5.91	5.07	7.45	
283	382626661	9.7	82.5	5250	3/16/20	4.61	4.97	5.52	7.51	
287	2758565	12.4	523.3	5807	7/17/19	4.85	5.57	5.25	6.80	
288	47316976	9.0	211.3	6530	7/16/19	5.46	7.95	5.28	8.53	
290	201233610	13.0	915.2	5736	7/20/19	4.47	5.23	4.98	6.28	False positive
291	49710555	12.3	552.4	5920	7/17/19	4.66	5.44	5.20	6.95	
					10/10/19	4.71	5.87	5.00	7.27	
294	188570092	11.4	126.8	4521	7/17/19	4.54	4.87	5.02	6.04	HATS-72
					9/12/19	4.87	5.46	5.16	7.25	
303	145750719	12.0	482.6	5659	7/18/19	4.56	5.12	5.01	6.20	HATS-60
306	114749636	11.8	464.5	5909	7/20/19	4.84	5.66	5.40	7.11	WASP-147
307	9100874	13.1	745.7	5747	7/15/19	4.60	5.36	5.29	6.59	
311	434105231	13.0	233.2	4063	10/10/19	4.63	5.32	4.77	6.71	False positive
313	9102327	11.3	313.4	5963	7/19/19	5.04	5.63	5.24	6.50	False positive
					10/10/19	5.27	6.82	5.40	8.19	
314	316769613	11.2	130.7	4822	7/20/19	5.35	6.70	5.17	8.04	
317	402319411	12.9	458.4	5391	7/20/19	4.77	5.90	4.92	7.30	
320	188593930	12.4	373.2	5913	7/17/19	4.76	5.53	5.48	7.05	False positive
329	169765334	10.7	285.6	5561	10/10/19	5.30	6.64	5.43	8.10	
331	262531275	13.0	950.5	5608	11/24/20	4.82	5.79	4.98	5.76	
344	13023378	11.9	403.5	6149	7/15/19	4.86	5.69	5.31	7.16	
353	100099031	13.5	1390.3	4965	1/14/20	4.36	4.81	5.04	6.26	
354	100097716	11.4	383.1	5767	11/24/20	5.10	6.03	4.91	6.27	
360	13023738	12.3	631.2	5657	7/15/19	4.76	5.71	5.46	7.36	
364	47425697	10.5	265.7	6220	7/16/19	4.91	5.77	4.83	7.28	
367	9033144	9.7	158.6	5757	7/19/19	5.51	6.50	5.47	7.26	False positive
372	441075486	12.0	516.0	5770	7/20/19	4.58	5.20	4.88	7.19	False positive
378	20892672	13.1	2316.4	5894	9/13/19	4.73	5.14	5.04	5.58	False positive
379	220396259	9.9	231.5	5825	11/25/20	4.81	5.18	5.16	6.45	False positive
380	100014359	13.5	400.2	5227	1/14/20	4.38	4.82	4.51	5.49	
391	382391899	11.1	182.3	5400	11/28/20	4.87	5.39	5.40	6.63	WASP-50
393	29960109	11.2	37.7	3450	9/12/19	4.66	5.30	5.30	7.36	False positive
398	1129033	9.6	105.7	5500	11/28/20	5.24	5.71	5.54	7.41	WASP-77

Table 4 *continued*

Table 4 *(continued)*

TOI	TIC	TESS Mag.	Distance (pc)	T_{eff} (K)	UT Date (MM/DD/YY)	ΔMag (562 nm) 0.2″	1.0″	ΔMag (832 nm) 0.2″	1.0″	Notes
402	120896927	8.3	44.9	5175	9/12/19	5.68	7.09	4.98	7.40	
403	257567854	11.2	317.1	6153	11/28/20	5.20	6.15	5.30	6.79	WASP-22
404	166833457	12.4	280.0	5473	11/30/20	4.79	5.12	5.14	6.19	WASP-98
411	100990000	7.8	62.9	6101	11/25/20	5.65	7.28	5.32	7.77	
436	44745077	13.1	77.4	3550	1/14/20	4.61	5.16	5.12	6.45	False positive
442	70899085	10.7	52.3	3779	1/14/20	4.44	4.89	5.48	7.23	
444	179034327	9.1	57.5	5229	1/9/20	5.11	6.72	5.53	8.17	
449	139528693	11.8	722.0	6291	11/24/20	5.24	6.12	5.26	6.85	WASP-78
452	139733308	11.9	247.0	5258	11/24/20	5.15	5.86	5.28	6.62	HATS-5
457	89256802	13.7	125.8	3054	1/14/20	4.63	5.03	4.61	5.32	
460	9804616	14.1	181.7	3274	1/10/20	4.55	4.80	4.57	5.69	False positive
465	270380593	10.7	121.8	4910	11/28/20	4.52	4.92	5.47	6.77	WASP-156
474	59843967	12.8	419.0	5403	11/26/20	4.70	5.11	5.13	5.95	HATS-4
486	260708537	9.4	15.2	3445	3/13/20	4.22	4.59	5.03	7.16	
487	31852980	9.8	157.8	5450	11/29/20	4.07	4.29	5.45	7.03	
500	134200185	9.4	47.4	4590	3/16/20	5.42	6.56	5.38	7.39	
507	348538431	13.2	109.9	3338	3/16/20	4.80	5.23	5.08	6.26	
525	71512186	8.8	152.8	7064	11/28/20	5.38	6.07	5.56	7.56	
536	234825296	13.9	891.6	5880	11/27/20	4.63	5.08	4.67	5.00	CoRoT-20
541	143271144	14.7	1121.1	4978	1/14/20	4.57	5.14	4.38	4.97	APC
542	49771092	14.8	952.6	5084	1/10/20	4.31	4.52	4.68	5.29	
545	37168957	14.2	783.1	5440	11/30/20	4.73	5.10	4.64	4.86	CoRoT-18
548	42821097	13.2	840.4	6090	11/30/20	4.77	5.09	4.43	4.97	CoRoT-19
555	170849515	14.9	395.2	3837	1/10/20	4.73	4.92	4.64	4.87	
562	413248763	8.7	9.4	3505	3/15/20	5.70	6.97	5.05	7.65	GJ 357
568	37575651	8.3	305.7	5780	1/8/20	5.26	6.15	4.58	6.78	
570	126733133	10.0	190.5	5973	1/11/20	5.17	5.70	5.27	7.12	
573	296780789	12.5	88.7	3400	3/15/20	4.65	5.18	4.82	6.34	TIC 876200724
584	74482749	9.1	412.8	9255	1/8/20	5.29	5.57	4.86	6.92	
586	131979339	8.2	249.6	9511	3/16/20	5.46	7.24	4.77	8.11	
593	128463355	10.1	384.8	6333	3/14/20	5.32	6.19	5.29	6.80	False positive
603	262746281	9.7	204.3	5901	3/16/20	4.61	5.31	5.00	7.70	
613	77527511	9.9	216.4	4949	3/16/20	4.88	5.76	4.82	7.46	
615	190496853	10.3	354.2	7437	1/11/20	5.20	6.29	5.14	7.26	
617	141227133	10.3	6813.8	2838	3/13/20	4.49	5.65	5.26	8.10	False positive
620	296739893	10.2	33.0	3630	3/16/20	4.83	5.79	4.68	8.01	
626	65412605	9.5	426.8	8489	5/18/19	3.65	4.84	5.24	7.03	False positive
633	348755723	13.9	116.5	3267	3/16/20	4.81	4.99	4.62	5.63	False positive
652	22221375	7.4	45.6	5903	3/15/20	5.77	7.74	5.24	7.93	HD 86226
663	54962195	11.8	63.9	3719	1/12/20	4.58	5.32	5.41	8.67	
674	158588995	11.9	46.2	3467	1/14/20	4.65	5.62	5.14	6.99	
687	74534430	9.8	42.4	4254	1/9/20	5.00	5.79	5.53	8.58	
695	55559618	10.7	144.7	5591	11/25/20	4.45	4.69	5.19	6.78	False alarm
697	77253676	9.4	92.9	5447	11/27/20	5.68	7.22	5.22	7.46	
700	150428135	10.9	31.1	3482	10/9/19	4.04	4.52	4.83	7.35	
702	237914496	11.8	84.4	4015	11/26/20	4.07	4.25	5.52	6.53	

Table 4 *continued*

Table 4 *(continued)*

TOI	TIC	TESS Mag.	Distance (pc)	$T_{\rm eff}$ (K)	UT Date (MM/DD/YY)	ΔMag (562 nm) 0.2″	1.0″	ΔMag (832 nm) 0.2″	1.0″	Notes
704	260004324	10.1	29.8	3625	10/9/19	4.74	6.43	4.68	7.99	LHS 1815
712	150151262	9.9	58.7	4504	1/10/20	4.29	5.04	5.56	7.81	
716	119081096	12.4	88.7	3776	3/13/20	4.83	5.40	5.15	6.27	False positive
717	275248683	11.4	34.4	3788	3/16/20	4.04	4.42	5.54	7.14	False positive
719	184952758	9.0	84.4	5653	3/16/20	5.62	6.96	5.36	8.05	False positive
721	38571020	10.2	206.3	6009	11/26/20	4.47	4.84	5.49	7.57	
722	38509907	11.9	116.2	4082	11/27/20	4.56	5.54	4.72	6.25	TIC 684936227
730	11561667	14.9	435.9	4105	1/10/20	4.47	4.75	4.54	5.08	
731	34068865	8.0	9.4	3518	1/10/20	4.67	4.93	4.48	4.77	
733	106402532	8.8	75.3	5969	3/15/20	5.18	6.98	5.08	7.71	
734	146846569	15.2	2843.9	3010	3/12/20	4.91	5.02	4.45	4.76	
738	260304800	12.7	390.6	5324	11/25/20	4.39	4.66	5.09	5.70	
741	359271092	7.7	5707.7	3766	1/11/20	4.53	4.79	5.37	7.16	
					1/14/20	4.78	5.40	5.18	9.13	
743	434486077	14.4	651.7	5156	1/10/20	4.48	4.86	4.68	5.23	
745	444842193	10.5	175.0	5741	1/11/20	4.94	5.46	5.21	7.16	
753	61988212	14.3	665.9	5591	3/12/20	4.86	5.18	4.59	4.91	False positive
754	72985822	12.2	514.2	6214	3/14/20	4.89	5.78	5.05	6.08	
755	73228647	9.5	105.8	6003	1/14/20	5.49	7.28	5.48	8.11	
756	73649615	12.6	86.1	3614	3/12/20	4.86	5.19	5.13	6.01	
761	165317334	10.9	66.5	4368	3/15/20	5.15	6.23	5.32	7.26	
762	178709444	13.7	98.8	3399	1/11/20	4.70	4.97	4.78	5.78	
763	178819686	9.5	95.6	5767	3/14/20	5.43	6.96	5.34	7.42	
776	306996324	9.7	27.2	3806	3/15/20	5.22	5.99	5.62	7.78	
777	334305570	9.4	179.4	7199	3/14/20	5.36	6.67	5.35	7.37	
778	335630746	8.7	162.6	6780	3/16/20	5.65	7.48	5.37	8.40	
783	451645081	9.9	55.5	4499	1/8/20	4.68	4.88	4.96	6.63	
784	460984940	8.8	64.6	5849	3/12/20	4.86	5.64	5.47	8.28	
791	306472057	10.8	336.5	6572	3/12/20	4.62	5.37	5.19	6.94	
797	271596225	11.7	56.1	3704	3/12/20	4.49	4.93	5.21	7.21	
798	260640693	11.9	121.1	4270	11/25/20	4.61	4.97	5.03	5.57	
805	38460940	13.1	51.9	3376	11/26/20	4.62	4.86	5.07	5.60	
					11/27/20	4.31	4.61	5.03	5.67	
808	30122649	10.1	97.2	5216	3/13/20	5.33	6.98	5.19	7.99	
813	55525572	9.8	262.9	5824	7/16/19	4.33	4.83	5.51	7.00	
815	102840239	9.4	59.4	4954	3/15/20	5.62	6.93	5.43	7.54	
823	158978373	10.0	205.7	6309	3/13/20	5.74	7.14	5.35	7.83	
824	193641523	10.1	63.9	4450	3/14/20	5.10	6.14	5.43	7.26	
829	276128561	10.6	138.9	5636	3/12/20	5.09	5.88	5.34	7.04	
833	362249359	10.1	41.8	3965	1/12/20	4.50	4.93	5.56	8.12	
835	405700729	10.8	166.6	6012	3/14/20	4.86	5.30	5.48	6.79	
836	440887364	8.6	27.5	4476	3/14/20	5.32	6.50	5.10	7.21	
838	461271719	8.8	319.3	7313	3/12/20	5.61	7.01	5.33	7.45	False positive
840	287563610	13.1	486.1	5318	3/12/20	4.83	5.40	5.04	5.51	
842	141768070	12.6	370.1	5376	1/10/20	4.50	4.53	5.00	5.69	
850	423670610	11.3	357.3	5864	9/12/19	5.01	5.23	5.27	6.27	APC

Table 4 *continued*

Table 4 *(continued)*

TOI	TIC	TESS Mag.	Distance (pc)	$T_{\rm eff}$ (K)	UT Date (MM/DD/YY)	ΔMag (562 nm) 0.2″	1.0″	ΔMag (832 nm) 0.2″	1.0″	Notes
851	40083958	11.0	169.6	5485	9/12/19	5.05	5.39	5.14	6.62	
854	160222069	10.7	276.4	5928	11/24/20	5.01	5.95	5.00	6.71	APC
858	198008005	10.6	251.7	5857	11/25/20	4.86	5.44	5.24	6.69	
860	321011127	11.7	505.1	5906	11/24/20	5.00	6.27	5.12	6.45	
863	238898571	10.0	111.4	5867	1/10/20	4.22	4.97	5.28	7.23	
866	381976956	9.0	448.1	4866	9/13/19	4.93	5.14	5.48	7.19	APC
					10/9/19	4.86	5.94	5.03	7.52	
870	219229644	10.8	53.8	3927	11/25/20	4.97	5.21	5.34	6.81	
873	237920046	12.1	77.2	3797	11/29/20	4.45	4.76	5.11	6.02	
879	37084932	9.5	532.1	8829	1/14/20	5.13	5.94	5.25	7.71	False positive
882	92013169	9.7	397.2	7069	11/30/20	4.09	4.33	5.27	6.90	
885	25334160	10.2	750.0	4313	1/14/20	4.96	6.13	5.06	8.31	APC
894	42755801	9.2	359.5	9900	1/14/20	4.97	6.39	4.98	7.60	False positive
896	102283403	9.1	155.5	6627	11/30/20	4.05	4.32	5.31	7.03	False alarm
897	229384040	9.1	164.0	6128	11/30/20	4.28	4.46	5.42	7.14	False positive
900	210873792	11.9	3262.1	3861	3/13/20	4.88	5.82	4.92	6.37	
902	216935214	9.0	224.3	7142	3/13/20	5.12	7.01	4.88	7.54	APC
905	261867566	10.6	157.2	5565	3/16/20	4.56	4.80	5.51	6.92	
906	298372701	8.5	135.4	5955	3/16/20	5.55	7.15	5.06	8.13	
907	305424003	9.9	303.5	6272	3/13/20	4.35	4.75	5.25	7.37	
912	406941612	10.5	635.4	3566	3/14/20	4.04	4.36	5.47	6.91	
913	407126408	9.6	65.0	4948	3/14/20	3.81	3.82	5.42	7.13	
919	150167117	11.2	330.4	5811	1/10/20	4.26	4.49	5.18	6.77	False positive
921	278775625	11.3	292.5	6056	3/16/20	4.69	5.70	5.42	7.54	
926	176796997	10.6	307.6	5658	11/28/20	4.73	6.21	5.30	6.78	
929	175532955	11.4	113.6	4451	11/24/20	5.13	6.07	5.42	6.84	
931	206474443	11.5	634.4	5928	1/12/20	4.33	5.54	4.96	6.88	
935	260476837	12.8	378.0	4814	1/8/20	4.63	4.71	4.55	4.87	False positive
938	332660150	10.8	213.1	5981	1/14/20	4.50	4.88	5.45	7.15	
939	67772767	10.9	349.3	6160	1/9/20	4.07	4.38	5.35	7.52	
950	245947683	10.2	209.6	6706	1/10/20	3.62	4.17	5.41	7.49	False alarm
952	319312479	10.1	417.1	7110	1/14/20	4.70	5.24	5.44	7.37	
954	44792534	9.8	239.1	5756	1/14/20	5.09	5.69	4.83	8.27	
964	179155220	10.7	126.4	5146	1/10/20	4.33	5.02	5.49	7.99	False positive
965	179159972	10.6	215.0	5948	1/10/20	4.42	5.25	5.39	8.00	False positive
969	280437559	10.5	77.8	4249	1/14/20	4.29	4.80	5.20	7.77	
974	333821572	10.4	502.6	8192	1/8/20	4.39	5.98	4.88	7.01	
976	347098457	10.5	3946.9	4240	1/8/20	4.19	5.26	4.67	6.91	False positive
994	93963408	10.0	524.9	10393	1/14/20	5.19	5.95	5.27	7.86	False positive
995	317951248	10.1	1249.0	4805	1/14/20	4.31	4.85	5.30	7.87	False positive
996	142918609	9.8	516.8	8007	1/14/20	5.02	7.02	4.70	7.62	False positive
998	54390047	9.7	514.9	8322	1/9/20	5.31	6.34	5.52	9.08	
1025	297967252	5.5	130.1	8599	1/11/20	5.95	7.17	5.33	7.70	
1028	447283466	7.9	23.7	4634	3/15/20	5.23	6.15	5.69	7.61	False positive
1031	304021498	9.7	270.6	6415	3/12/20	4.41	4.92	5.53	7.66	False positive
1032	146589986	9.8	598.9	10395	1/11/20	5.65	6.83	5.00	7.76	

Table 4 *continued*

Table 4 *(continued)*

TOI	TIC	TESS Mag.	Distance (pc)	T_{eff} (K)	UT Date (MM/DD/YY)	ΔMag (562 nm) 0.2″	1.0″	ΔMag (832 nm) 0.2″	1.0″	Notes
1034	400595342	9.8	349.3	9810	1/8/20	5.41	5.77	5.25	6.93	False positive
1035	361413119	10.1	365.1	5964	1/12/20	4.37	4.88	4.85	7.32	466 + 617 nm filters
1036	146172354	10.3	182.8	5771	1/11/20	5.43	6.41	5.60	7.99	
1037	363260203	9.0	274.8	9158	3/12/20	5.53	6.39	5.28	8.16	
1038	90544017	8.7	252.0	8904	1/14/20	4.99	7.54	4.64	8.44	False positive
1039	461867584	8.5	1523.9	15000	1/9/20	4.55	5.08	4.79	7.01	APC
1041	385624852	8.1	296.5	9081	3/12/20	5.25	6.91	5.19	7.59	False positive
1042	360286627	9.7	801.5	9917	3/12/20	4.95	5.36	5.15	7.65	
1047	370745311	10.2	135.3	5622	1/12/20	4.48	5.11	5.11	7.04	False positive
1048	384549882	8.8	446.1	11892	3/12/20	5.44	6.79	5.28	7.75	False positive
1051	259863352	7.1	63.1	5625	11/26/20	4.55	4.97	5.22	7.53	False alarm
1062	299799658	9.5	82.3	5394	1/14/20	4.39	4.74	5.08	8.19	
1063	406976746	9.1	61.3	5552	3/14/20	4.20	4.34	4.93	6.59	
1064	79748331	10.0	68.7	4803	9/12/19	5.12	6.00	5.48	7.74	
1078	370133522	10.1	20.4	3325	9/13/19	4.70	4.79	5.16	6.72	GJ 1252
					9/16/19	4.43	4.84	5.31	7.37	
					9/28/19	4.63	5.35	5.72	8.13	
					10/10/19	4.46	5.39	5.05	8.87	
1089	129319156	10.4	717.8	11600	3/14/20	4.92	6.43	5.48	7.36	False positive
1091	193413306	9.4	313.4	7348	3/13/20	5.24	6.26	5.45	8.35	
1092	387079085	9.0	211.0	6534	3/13/20	4.72	5.24	5.26	7.52	False positive
1093	382331352	10.0	592.6	4000	3/13/20	4.68	5.33	5.47	7.57	False positive
1094	136274063	10.0	358.9	7710	3/14/20	5.13	5.84	5.21	7.21	False positive
1097	360630575	8.7	79.6	5876	3/13/20	4.65	5.18	5.41	8.10	
1098	383390264	8.8	105.1	6153	1/14/20	3.74	4.18	5.28	6.94	
1099	290348383	7.4	24.4	4867	9/28/19	5.06	5.85	5.29	8.31	
1202	327017634	8.4	927.9	3773	3/14/20	4.72	5.49	5.07	7.19	False positive
1204	467666275	8.0	106.4	6711	1/8/20	5.09	5.26	6.10	7.36	
1211	50312495	9.8	127.6	5573	11/29/20	4.09	4.32	5.53	7.20	
1217	248092710	9.7	472.4	6354	3/14/20	5.54	6.94	5.59	7.89	
1227	360156606	13.8	101.0	3050	3/13/20	4.02	4.30	4.99	5.49	
1231	447061717	10.3	27.5	3540	3/15/20	4.70	5.82	6.04	7.47	
1233	260647166	8.7	64.6	5724	1/14/20	4.97	6.61	4.83	7.28	
					3/12/20	5.75	6.67	5.58	7.80	
1478	409794137	10.2	152.3	5623	1/14/20	4.99	6.90	4.72	8.52	
1915	98283926	13.1	808.0	6208	11/29/20	4.78	5.33	4.84	5.29	HATS-42
2008	70887357	8.6	136.6	5463	11/30/20	5.70	7.01	5.50	7.27	
2179	237913194	11.5	307.8	5695	11/29/20	4.72	4.97	5.41	6.60	
2195	24695044	11.0	175.3	5296	11/27/20	3.88	4.06	5.33	6.64	
2202	358107516	12.2	236.6	5064	11/27/20	3.84	4.18	5.11	6.41	
2208	38680052	15.7	183.1	3228	11/29/20	4.39	4.55	4.46	4.78	
2212	280803917	12.4	315.6	5234	11/26/20	4.07	4.45	5.26	6.29	
					11/27/20	4.26	4.60	5.23	6.22	
2217	234330672	12.8	699.5	5987	11/27/20	4.23	4.57	5.08	5.95	
2220	150437346	11.7	354.9	5810	11/25/20	4.48	4.76	5.16	6.09	
2235	267093376	10.9	399.5	6378	11/26/20	3.90	4.17	5.25	6.85	APC

Table 4 *continued*

Table 4 *(continued)*

TOI	TIC	TESS Mag.	Distance (pc)	$T_{\rm eff}$ (K)	UT Date (MM/DD/YY)	ΔMag (562 nm) 0.2″	1.0″	ΔMag (832 nm) 0.2″	1.0″	Notes
2239	388130235	10.8	456.5	5030	11/29/20	4.67	5.07	5.62	7.27	
2305	232079930	12.8	584.7	5582	11/26/20	3.95	4.41	4.97	5.79	APC
					44164	4.14	4.47	4.90	5.36	
2310	38467100	13.0	923.3	5266	44164	4.67	5.25	4.45	5.34	

REFERENCES

Astropy Collaboration, Robitaille, T. P., Tollerud, E. J., et al. 2013, A&A, 558, A33. doi:10.1051/0004-6361/201322068

Astropy Collaboration, Price-Whelan, A. M., Sipőcz, B. M., et al. 2018, AJ, 156, 123. doi:10.3847/1538-3881/aabc4f

Borucki, W. J., Koch, D., Basri, G., et al. 2010, Science, 327, 977

Ciardi, D. R., Beichman, C. A., Horch, E. P., et al. 2015, ApJ, 805, 16

Cieza, L. A., Padgett, D. L., Allen, L. E., et al. 2009, ApJL, 696, L84. doi:10.1088/0004-637X/696/1/L84

Colton, N. M., Horch, E. P., Everett, M. E., et al. 2021, AJ, 161, 21. doi:10.3847/1538-3881/abc9af

Dawson, R. I. & Johnson, J. A. 2018, ARA&A, 56, 175. doi:10.1146/annurev-astro-081817-051853

Duquennoy, A. & Mayor, M. 1991, A&A, 500, 337

Fontanive, C., Rice, K., Bonavita, M., et al. 2019, MNRAS, 485, 4967. doi:10.1093/mnras/stz671

Furlan, E., Ciardi, D. R., Everett, M. E., et al. 2017, AJ, 153, 71. doi:10.3847/1538-3881/153/2/71

Gaia Collaboration, Prusti, T., de Bruijne, J. H. J., et al. 2016, A&A, 595, A1

Gaia Collaboration, Brown, A. G. A., Vallenari, A., et al. 2020, arXiv:2012.01533

Harris, C. R., Millman, K. J., van der Walt, S. J., et al. 2020, Nature, 585, 357. doi:10.1038/s41586-020-2649-2

Hirsch, L. A., Rosenthal, L., Fulton, B. J., et al. 2021, AJ, 161, 134. doi:10.3847/1538-3881/abd639

Holman, M. J. & Wiegert, P. A. 1999, AJ, 117, 621. doi:10.1086/300695

Horch, E. P., Gomez, S. C., Sherry, W. H., et al. 2011, AJ, 141, 45

Horch, E. P., Howell, S. B., Everett, M. E., et al. 2014, ApJ, 795, 60

Howell, S. B., Everett, M. E., Sherry, W., et al. 2011, AJ, 142, 19

Howell, S. B., Sobeck, C., Haas, M., et al. 2014, PASP, 126, 398

Howell, S. B., Scott, N. J., Matson, R. A., et al. 2019, AJ, 158, 113. doi:10.3847/1538-3881/ab2f7b

Howell, S. B., Matson, R. A., Ciardi, D. R., et al. 2021, AJ, 161, 164. doi:10.3847/1538-3881/abdec6

Hunter, J. D. 2007, Computing in Science and Engineering, 9, 90. doi:10.1109/MCSE.2007.55

Jang-Condell, H. 2015, ApJ, 799, 147. doi:10.1088/0004-637X/799/2/147

Kraus, A. L., Ireland, M. J., Hillenbrand, L. A., et al. 2012, ApJ, 745, 19. doi:10.1088/0004-637X/745/1/19

Kraus, A. L., Ireland, M. J., Huber, D., et al. 2016, AJ, 152, 8

Malkov, O. Y. 2007, MNRAS, 382, 1073. doi:10.1111/j.1365-2966.2007.12086.x

Martin, R. G., Nixon, C., Lubow, S. H., et al. 2014, ApJL, 792, L33. doi:10.1088/2041-8205/792/2/L33

Matson, R. A., Howell, S. B., Horch, E. P., et al. 2018, AJ, 156, 31

Matson, R. A., Howell, S. B., & Ciardi, D. R. 2019, AJ, 157, 211

Moe, M. & Kratter, K. M. 2019, arXiv:1912.01699

Mugrauer, M. & Michel, K.-U. 2020, Astronomische Nachrichten, 341, 996. doi:10.1002/asna.202013825

Musielak, Z. E., Cuntz, M., Marshall, E. A., et al. 2005, A&A, 434, 355. doi:10.1051/0004-6361:20040238

Pecaut, M. J., Mamajek, E. E., & Bubar, E. J. 2012, ApJ, 746, 154. doi:10.1088/0004-637X/746/2/154

Pecaut, M. J. & Mamajek, E. E. 2013, ApJS, 208, 9

Quintana, E. V., Lissauer, J. J., Chambers, J. E., et al. 2002, ApJ, 576, 982. doi:10.1086/341808

Raghavan, D., McAlister, H. A., Henry, T. J., et al. 2010, ApJS, 190, 1

Ricker, G. R., Winn, J. N., Vanderspek, R., et al. 2015, JATIS, 1, 014003

Savel, A. B., Dressing, C. D., Hirsch, L. A., et al. 2020, AJ, 160, 287. doi:10.3847/1538-3881/abc47d

Scott, N. J., Howell, S. B., Horch, E. P., et al. 2018, PASP, 130, 054502

Scott, N. J., et al. 2021, *in preparation*

Stassun, K. G., Oelkers, R. J., Pepper, J., et al. 2018, AJ, 156, 102. doi:10.3847/1538-3881/aad050

Stassun, K. G., Oelkers, R. J., Paegert, M., et al. 2019, AJ, 158, 138. doi:10.3847/1538-3881/ab3467

Virtanen, P., Gommers, R., Oliphant, T. E., et al. 2020, Nature Methods, 17, 261. doi:10.1038/s41592-019-0686-2

Wang, J., Fischer, D. A., Xie, J.-W., et al. 2014, ApJ, 791, 111. doi:10.1088/0004-637X/791/2/111

Winters, J. G., Henry, T. J., Jao, W.-C., et al. 2019, AJ, 157, 216

Ziegler, C., Tokovinin, A., Briceño, C., et al. 2020, AJ, 159, 19

Ziegler, C., Tokovinin, A., Latiolais, M., et al. 2021, arXiv:2103.12076